International Journal of Engineering Trends and Technology
ISSN: 2231–5381 / https://doi.org/10.14445/22315381/IJETT-V71I4P236

Volume 71 Issue 4, 416-435, April 2023

Original Article

A Multi-Mode Approach to Geometrically Nonlinear Free and Forced Vibrations of Rectangular Plate Resting on Two Line Supports

Ahmed Babahammou[1], Rhali Benamar[1]

[1]*University Mohammed V in Rabat, E.M.I. BP 765, Rabat, Morocco.*

[1]*Corresponding Author : ahmedbabahammou@gmail.com*

Received: 02 February 2023 Revised: 04 April 2023 Accepted: 12 April 2023 Published: 25 April 2023

Abstract *- Linear and geometrically nonlinear free and forced vibrations analysis by the multi-mode approach of continuous rectangular plates is performed by a semi-analytical method. The Rayleigh-Ritz method is used to calculate the linear frequency parameters and associated mode shapes. The line supports are modeled by distributions of translational springs contributing to the plate strain energy with a stiffness tending to infinity. The choice of the trial functions set presents the novelty of this work. Indeed, this set does not respect the intermediate lines but must only verify the plat boundary conditions. The linear results found are compared to those of previous work to verify the accuracy and reliability of the present formulation. On the other hand, Benamar's method is used to investigate the nonlinear vibrations of the studied plate. A code is performed for this work to use the lsqnonlin routine from Matlab software. This code solves the nonlinear algebraic system using the least squares method. The plotted backbone curves show that the hardening type of the studied plate admits a minimum function of the aspect ratio. The amplitude-dependent nonlinear mode shapes are plotted and discussed. The forced regime was investigated by concentrated and distributed harmonic excitation forces with several levels.*

Keywords *- Rectangular plates, Intermediate lines, Nonlinear vibrations, Free and forced regime, Bending stress.*

1. Introduction

Buildings, bridges, airplanes, and marine engineering structures are examples of plates that can model with line supports, sometimes called continuous or multi-span plates. The analysis of the dynamic behavior of this type of plate aims to minimize the vibratory responses and optimize the distribution of stresses during external excitations due to machine movement, vehicle circulations, etc. Moreover, in the absence of intermediate lines, the plates may undergo significant deformation resulting in structural failure.

The linear vibrations of continuous plates were investigated by many theories since the early Holzer method of Veletsos and Newmark, [1] the semi-graphical approach treated by Ungar [2], the edge effect approach developed by Bolotin [3] and Moskalenko [4], the finite strip method used by Cheung [5], the modified Bolotin method employed by Elishakoff [6] and the receptance method studied by Azimi [7]. Moreover, the Rayleigh-Ritz method analyzed were used to analyze the linear vibration of the continuous plate by several researchers using different type of trial beam functions: Dickinson [8] used a set of one-dimensional orthogonal polynomial functions, Mizusawa [9] used the B-spline functions, Wu and Cheung [10] used the multi-span vibrating beam functions, Liew and Lam [11] used a set of two-dimensional orthogonal polynomial functions, Kong and Cheung [12] combined this set of trial functions, Cheung and Kong [13] used the finite strip method and Zhou [14,15] proposed the single-span vibrating beam functions plus augmented polynomials as a set of beam functions.

Several recent research pieces have investigated these plates' linear vibration with more complication. Zhou [16] treated the continuous Midline plates by the Rayleigh-Ritz method using static Timoshenko beam functions. Xiang [18] developed the discrete singular convolution method to analyze the plates with partial internal supports. C.F.Lü [19] studied the generally supported Kirchhoff plates by the state-space-based differential quadrature method. Rezaiguia [20,21] developed a new semi-analytical method to determine the natural frequencies and mode shapes of multi-span bridge decks, and M. Huang [22] investigated the continuous plates with partial line support. Topal [23] optimized the frequency of laminated composite plates with different intermediate line supports. Tiangui and wang [24,50] used a modified Fourier solution for analyzed the vibrations of moderately thick laminated continuous plates. Rezaiguita et al. [26,27] analyzed continuous orthotropic bridge decks by a semi-analytic method.

Despite a large amount of research already carried out on the continuous plates, it appears that the geometrically nonlinear vibration of continuous plates has not been investigated yet, to the best of the author's knowledge.

On the other hand, Benamar's team has studied the nonlinear vibrations of plates, shells and beams numerically [29-39,51], using an iterative solution based on the Harwell NS01A library routine, which was programmed by the FORTRAN software. However, some works performed by this team [40-47] used approximate solutions for the

nonlinear vibration of structures. These approximate solutions, developed by El Kadiri and Benamar [30], are valid just for low amplitudes.

The present work aims to study a three-span plate's geometrically nonlinear free and forced vibrations using a multi-mode approach without approximate solutions. First, the Rayleigh-Ritz method performed in the present work uses a new set of trial beam functions. In fact, these latter do not have to respect the intermediate lines; they have to verify the end conditions. These end conditions allow for finding a system of 4 equations and five unknowns. The nullity of the determinant of this system allows determining the beam frequency parameters to calculate and plot the trial beam functions. It should be mentioned that the chosen set of trial beam functions makes it easy to achieve a stable calculation and gives a rapid convergence for the vibration plate calculations. Secondly, the kinetic, the linear strain energy due to the bending, and the strain membrane energy due to the large amplitude are calculated, discretized, and derived. Hamilton's principle was applied to lead the nonlinear system governing the motion of the continuous plate. In this system, the contribution of the membrane energy is neglected for studying the linear vibrations. An accurate convergence study was carried out. The numerical results were obtained via eigenvalue, and the linear mode shapes were calculated and plotted. Thirdly, Benamar's method was applied to solve the nonlinear system. Residuals were calculated to verify the accuracy of the solution. The effect of the line supports and the aspect ratio on the fundamental nonlinear mode shapes was illustrated by the mode shapes and the backbone curves. In the forced nonlinear regime, both concentrated and distributed harmonic forces were treated end illustrated by nonlinear forced frequency response functions in the vicinity of the fundamental mode. The effects of the variation in excitation level and the aspect ratio of the studied plate were investigated and illustrated.

2. General Formulation

The three-span plate in one direction studied in the present work is shown in Figure 1. a, b and H are its length, width, and thickness, respectively. Its mechanical characteristics are Young's modulus E, Poisson's ratio ν (in all follows $\nu = 0.3$), a mass density per unit area ρ, and a flexural rigidity $D = \frac{EH^3}{12(1-\nu^2)}$. It is supported by two intermediate lines parallel to the y-direction at $x_1 = \frac{a}{4}$ and $x_2 = \frac{3a}{4}$.

2.1. Trial Functions

This work is based on the Rayleigh-Ritz in the linear vibration and Benamar's methods in the nonlinear case. The convergence and accuracy of these methods strongly depend on the good choice of the beam functions used. This section exposes the trial plate and beam functions used.

As in the classical studies of plate vibrations, a current point $M(x, y)$ of the middle plane has a deflection $W(x, y, t)$ dependent on space and time. This deflection is based on the assumptions of the separation of time and space and the harmonic motion:

$$W(x, y, t) = w(x, y)\sin(\omega t) \tag{1}$$

ω is the vibration frequency, and the space function $w(x, y)$ is assumed to be expanded as a series of N basic functions $w_k(x, y)$ [29,30,51]:

$$w(x, y) = a_k w_k(x, y) \quad k = 1..N \tag{2}$$

The repeat index indicates the usual summation convention a_k is the basic function contribution coefficient of the k^{th} trial plate function w_k. This latter is assumed to be the product of the i^{th} beam function $X_i(x)$ in the x-direction and the j^{th} beam function $Y_i(y)$ in the y-direction:

$$w_k(x, y) = X_i(x)Y_j(y) \quad \text{with} \quad k = n(i-1) + j \tag{3}$$

In which $X_i(x)$ and $Y_j(y)$ are the trial beam functions that have the same plate boundary conditions in the x-and y-direction, respectively, they are expressed by [51]:

$$\begin{aligned} X_i(x) &= \sin(\bar{\omega}_{x,i}x) + C_{x1}\cos(\bar{\omega}_{x,i}x) + C_{x2}\sinh(\bar{\omega}_{x,i}x) + C_{x3}\cosh(\bar{\omega}_{x,i}x) \quad 0 \le x \le a, \quad i = 1 \dots m \\ Y_j(y) &= \sin(\bar{\omega}_{y,j}y) + C_{y1}\cos(\bar{\omega}_{y,j}y) + C_{y2}\sinh(\bar{\omega}_{y,j}y) + C_{y3}\cosh(\bar{\omega}_{y,j}y) \quad 0 \le y \le b, \quad j = 1 \dots n \end{aligned} \tag{4}$$

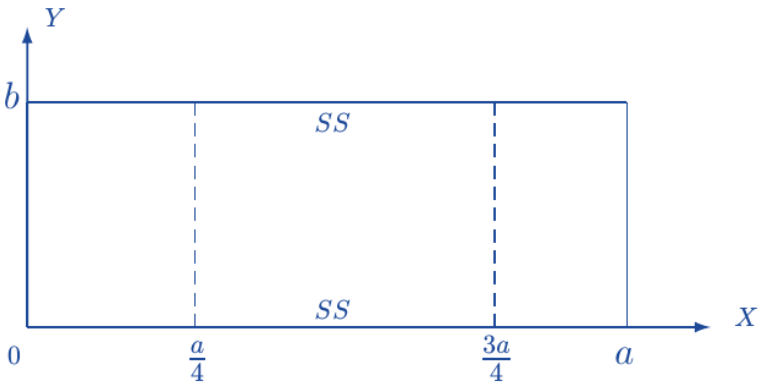

Fig. 1 The three-span rectangular studied plate

Where $\bar{\omega}_{x,i}$ and $\bar{\omega}_{y,j}$ are the i^{th} and j^{th} the natural frequency of the beam in the x- and y-direction, respectively. They are determined using the end conditions by calculating the nullity of the determinant of the system due to the end conditions. This latter also makes it possible to calculate the integration constants C_{x1},C_{x2}, C_{x3},C_{y1}, C_{y2} and C_{y3}. The novelty of the present work is that the beam functions should only verify the end conditions that are identical to the plate boundary conditions.

Table 1. The first fourteen frequency parameters $\lambda = \frac{\bar{\omega}}{\pi}$ of S.S., SC and CC beams.

	λ_1	λ_2	λ_3	λ_4	λ_5	λ_6	λ_7	λ_8	λ_9	λ_{10}
SS	1.0000	2.00	3.00	4.00	5.00	6.00	7.00	8.00	9.00	10.00
SC	1.2499	2.25	3.25	4.25	5.25	6.25	7.25	8.25	9.25	10.25
CC	1.5056	2.50	3.50	4.50	5.50	6.50	7.50	8.50	9.50	10.50

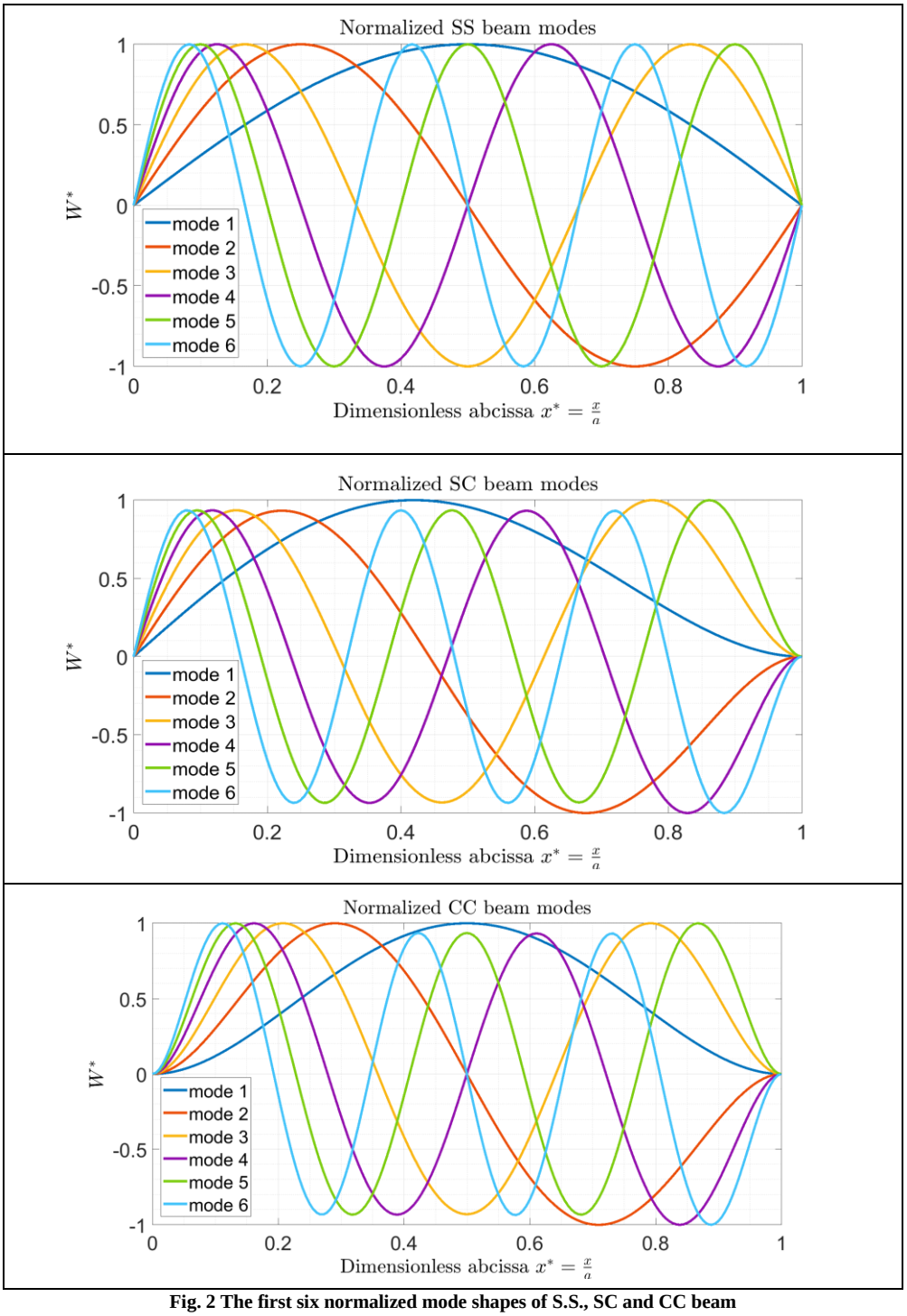

Fig. 2 The first six normalized mode shapes of S.S., SC and CC beam

The presence of line supports takes into account the energy calculation studied below.

The number of the trial plate functions is $N = n \times m$, and m and n are the number of the beam functions in the x and y-direction, respectively. For illustration, the ten lowest frequency parameters $\lambda_i = \frac{\omega_i}{\pi}$ of S.S., SC and CC beam are listed in Table 1. Furthermore, the first six symmetrical and asymmetrical mode shapes of the same beams are plotted in Figure 2.

Figure 2 shows that these beam functions do not consider any intermediate line inside the plate, and the slopes are zero at the clamped ends. The choice of beam functions, $X_i(x)$ and $Y_j(y)$ It is quite easy since they do not have to verify the conditions imposed by the presence of intermediate lines but only to respect the appropriate end conditions. The zero deflection at the intermediate lines is guaranteed by the strain energy of the translational spring distributions, with the stiffness tending to infinity.

2.2. Energies Study

The plate kinetic energy T is expressed as in [29-32,51]:

$$T = \frac{1}{2}\rho H \int_S \left(\frac{\partial W}{\partial t}\right)^2 dS \tag{5}$$

The strain energy V_b due to the bending is given by [51]:

$$V_b = \frac{D}{2}\int_S \left(\frac{\partial^2 W}{\partial x^2} + \frac{\partial^2 W}{\partial y^2}\right)^2 + 2(1-\nu)\left(\left(\frac{\partial^2 W}{\partial x\,\partial y}\right)^2 - \frac{\partial^2 W}{\partial x^2}\frac{\partial^2 W}{\partial y^2}\right) dS \tag{6}$$

The membrane strain energy V_m, induced by the large vibration amplitudes is expressed: [51]

$$V_m = \frac{3D}{2H^2}\int_S \left[\left(\frac{\partial W}{\partial x}\right)^2 + \left(\frac{\partial W}{\partial y}\right)^2\right]^2 dS \tag{7}$$

The two-line supports are modeled by fictitious translational spring distributions with infinite rigidity K_y in order to eliminate the transversal displacement at each point of these lines. Practically, the rigidity of the above spring distributions takes a very great value (10^{10}). Hence, the strain energy stored by the intermediate lines V_L is expressed by:

$$V_L = \frac{1}{2}\sum_{i=1}^{2} \int_0^b K_y\big(W(x_i, y)\big)^2 dy \tag{8}$$

The total plate strain energy V is the sum of the above strain energies:

$$V = V_b + V_L + V_m \tag{9}$$

By replacing Equation 2 in Equations 5 to 8, the discretization of the above energies is found and expressed by:

$$\begin{aligned} T &= \frac{1}{2}\omega^2 a_i a_j m_{ij}\cos^2(\omega t) \\ V_b &= \frac{1}{2}a_i a_j k_{ij}^b \sin^2(\omega t) \\ V_m &= \frac{1}{2}a_i a_j a_k a_l b_{ijkl}\sin^4(\omega t) \\ V_L &= \frac{1}{2}a_i a_j k_{ij}^L \sin^2(\omega t) \end{aligned} \tag{10}$$

In which m_{ij} , k_{ij}^b, b_{ijkl} are the general term of the mass, the linear rigidity and the nonlinear rigidity tensors, respectively. k_{ij}^L is the general term of the rigidity tensor associated with the energy stored in the intermediate lines supposed to be elastic. These tensors are expressed by:

$$\begin{aligned} m_{ij} &= \rho H \int_S w_i w_j dS \\ k_{ij}^b &= D\int_S \left(\frac{\partial^2 w_i}{\partial x^2} + \frac{\partial^2 w_i}{\partial y^2}\right)\left(\frac{\partial^2 w_j}{\partial x^2} + \frac{\partial^2 w_j}{\partial y^2}\right) + 2(1-\nu)\left(\frac{\partial^2 w_i}{\partial x\,\partial y}\frac{\partial^2 w_j}{\partial x\,\partial y} - \frac{\partial^2 w_i}{\partial x^2}\frac{\partial^2 wj}{\partial y^2}\right) dS \\ b_{ijkl} &= \frac{3D}{H^2}\int_S \left(\frac{\partial w_i}{\partial x}\frac{\partial w_j}{\partial x} + \frac{\partial w_i}{\partial y}\frac{\partial w_j}{\partial y}\right)\left(\frac{\partial w_k}{\partial x}\frac{\partial w_l}{\partial x} + \frac{\partial w_k}{\partial y}\frac{\partial w_l}{\partial y}\right) dS \\ k_{ij}^L &= \sum_{i=1}^{2}\int_0^b \left(K_y w_i w_j\right)_{x=x_i} dy \end{aligned} \tag{11}$$

one puts k_{ij} the general term of the plate linear rigidity tensor, which is the sum of the general terms of the rigidity tensor due to the bending and the tensor of the strain energy stored in the line supports:

$$k_{ij} = k_{ij}^b + k_{ij}^L \tag{12}$$

The vibration problem is governed by Hamilton's principle [51]:

$$\delta \int_0^{\frac{2\pi}{\omega}} (V - T)dt = 0 \tag{13}$$

As mentioned above, V and T are the total strain and kinetic energies of the studied plate. That leads to a nonlinear system, written in a matrix form as [29,30,51].

$$2[K]\{A\} + 3[B\{A\}]\{A\} - 2\omega^2[M]\{A\} = \{0\} \tag{14}$$

Where $\{A\} = \{a_1\ a_2 \dots a_N\}^T$ the column vector of the basic function contribution coefficients is$[M]$,$[K]$ $[B\{A\}]$ are the matrices associated with the tensors defined above. Equation 14 depends implicitly on the geometrical and mechanical plate characteristics and leads to not very exploitable results. In order to make the results more general, a dimensionless formulation is necessary. To write Equation 14 in a dimensionless form, the above tensors and the other parameters of this study must be replaced by their corresponding dimensionless form denoted by * in the exponent and defined by:

$$\frac{x}{x^*} = a, \qquad \frac{y}{y^*} = b, \qquad \frac{w}{h^*} = H, \qquad \frac{K_y}{K_y^*} = \frac{D}{a^3},$$

$$\frac{m_{ij}}{m_{ij}^*} = ab\rho h^3, \quad \frac{k_{ij}^b}{k_{ij}^{*b}} = \frac{bH^2D}{a^3}, \quad \frac{k_{ij}^L}{k_{ij}^{*L}} = \frac{bH^2D}{a^3}, \quad \frac{b_{ijkl}}{b_{ijkl}^*} = \frac{bH^2D}{a^3} \tag{15}$$

The dimensionless parameters defined in Equation 15 lead to the main parameter to be found in this study which is the dimensionless frequency parameter Ω such as:

$$\Omega^2 = a^4 \frac{\rho H}{D} \omega^2 \tag{16}$$

By replacing Equation 15 in Equation 14, one obtains the dimensionless motion equation of the transverse vibrations of the plate with line supports:

$$2[K^*]\{A\} + 3[B^*\{A\}]\{A\} - 2\Omega^2[M^*]\{A\} = \{0\} \tag{17}$$

$[M^*]$ is the dimensionless mass matrix, its general term is defined by:

$$m_{ij}^* = \int_{S^*} w_i^* . w_j^* dS^* \tag{18}$$

in which $S^* = x^* \times y^*$ is the dimensionless plate area $[0,1] \times [0,1]$, and $dS^* = dx^* \times dy^*$ is the dimensionless elementary area.

$[K^*] = [K^*]^b + [K^*]^L$ is the dimensionless linear rigidity matrix, in which $[K^*]^b$ is the dimensionless rigidity matrix due to the bending. Its general term is defined by:

$$k_{ij}^{*b} = \int_{S^*} \frac{\partial^2 w_i^*}{\partial x^{*2}} \frac{\partial^2 w_j^*}{\partial x^{*2}} + \alpha^2 \left(\frac{\partial^2 w_i^*}{\partial x^{*2}} \frac{\partial^2 w_j^*}{\partial y^{*2}} + \frac{\partial^2 w_i^*}{\partial y^{*2}} \frac{\partial^2 w_j^*}{\partial x^{*2}} \right) + \alpha^4 \frac{\partial^2 w_i^*}{\partial y^{*2}} \frac{\partial^2 w_j^*}{\partial y^{*2}} + 2(1-\nu)\alpha^2 \left(\frac{\partial^2 w_i^*}{\partial x^* \partial y^*} \frac{\partial^2 w_j^*}{\partial x^* \partial y^*} - \frac{\partial^2 w_i^*}{\partial x^{*2}} \frac{\partial^2 w_j^*}{\partial y^{*2}} \right) dx^* dy^* \tag{19}$$

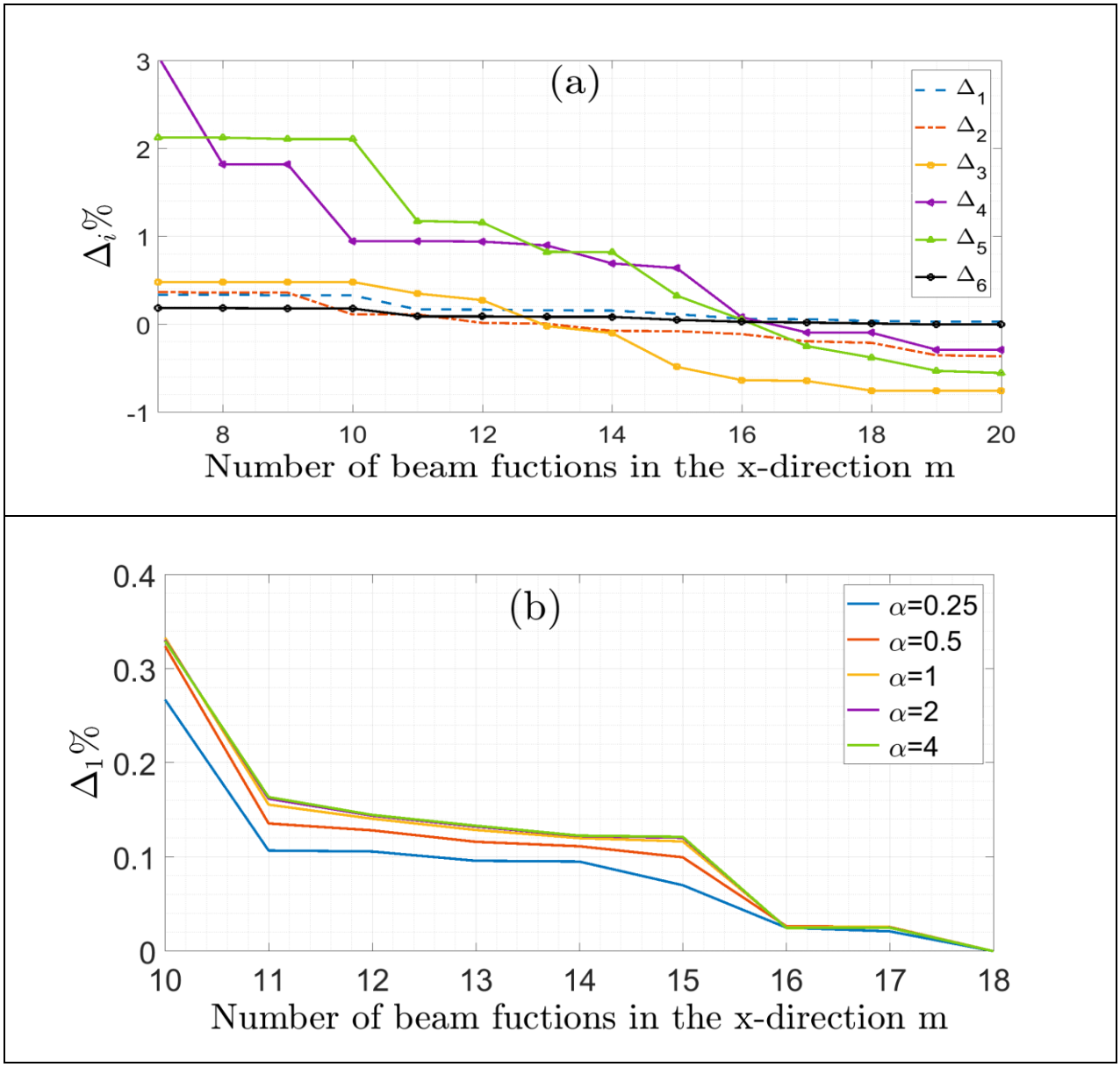

Fig. 3 Convergence study of a continuous CCSS studied plate: (a) studding the six lowest frequency parameters Ω_i for $\alpha = 4$, (b) studding the first frequency parameters for several values of the aspect ratio $\alpha = 0.25, 0.5, 1, 2, 4$.

where $\alpha = \frac{a}{b}$ is the plate aspect ratio and $[K^*]^L$ is the dimensionless rigidity matrix associated with the strain energy stored in the fictitious translational spring distributions which model the line supports. Its general term is defined by:

$$k_{ij}^{*L} = \int_0^1 K_y^*\left(w_i^*(x_1, y^*)w_j^*(x_1, y^*)\right)dy^* + \int_0^1 K_y^*\left(w_i^*(x_2, y^*)w_j^*(x_2, y^*)\right)dy^* \quad (20)$$

Equation 17 presents the motion equation of the nonlinear vibration problem, which must be solved numerically. Its solution yields the frequency parameters Ω_k expressed in Equation 16, as well as the mode shapes w_k described in Equation 2 for $k = 1$ to N.

3. Results Validation for Linear Vibration

In the linear analysis performed first, the fourth-order tensor $[B^*]$ Equation 17 is neglected; one gets the classical eigenvalue problem:

$$2[K^*]\{A\} - 2\Omega^2[M^*]\{A\} = \{0\} \quad (21)$$

Equation 21 has been solved numerically using a Matlab software code performed for the present work. This code analyses the effects of the number and locations of the line supports as well as the aspect ratio $\alpha = \frac{a}{b}$ of the continuous plate on the frequency parameters and mode shapes. A clamped (C) and simply-supported (S) are the boundary conditions considered for the three-span rectangular studied plates.

The boundary conditions of the plates in the present article are designed by four capital letters, the first two letters designate the edges $x = 0$ and $x = a$, and the last two letters designate the edges $y = 0$ and $y = b$. The values of the linear frequency parameters Ω for the six lowest vibration modes are calculated and compared to those available in the literature.

3.1. Convergence study

The convergence of the solution based on the proposed Rayleigh-Ritz formulation, expressed by Equation 21, is carried out for a three-span CCSS rectangular plate, having an aspect ratio $\alpha = 4$ and two intermediate lines at $X_1 = 0.25$ and $x_2 = 0.75$. Considering the simply supported edges in the y-direction and for uniformity of computation with the results taken as reference, two trial beam functions are used in this direction. The relative differences, denoted $\Delta_i\%$, between the six lowest frequency parameters $\Omega_i = b^2\sqrt{\frac{\rho H}{D}}\omega_i$ found in the present work, and the six frequency parameters taken as references Ω_{ref_i}, are defined by:

$$\Delta_i\% = \frac{\Omega_i - \Omega_{ref_i}}{\Omega_{ref_i}} \times 100 \quad i = 1 \ to \ 6 \quad (22)$$

It is well known that the Raileigh-Ritz method gives upper bounds to the exact results, so the frequency parameters given by Zhou [16] are taken as references Ω_{ref_i} because they are the small results in the bibliography found by the R.R.M.

The convergence study of the six lowest frequency parameters is shown in Figure (3. a). This latter Figure gives the curves of the relative differences Δ_i versus m the number of the trial beam functions in the x-direction varies from 7 to 20. From m = 13, some present results are lower than the reference and, therefore Δ_i becomes negative, i.e., the present results are more accurate than those given in the bibliography. The value $m = 16$ seems to be optimal since the relative differences Δ_i remains less than 0.7% for the first six frequency parameters. The convergence study of the first frequency parameters for several values of the aspect ratio α is performed using Figure 3. b. The Figures for the other six lowest frequency parameters are very similar to Figure (3. b); they are omitted for brevity. One can be concluded that the convergence study is insensitive to the aspect ratio. For $m = 16$ trial beam functions in the x-direction and $n = 2$ trial beam functions in the y-direction, the coefficient contributions a_k, listed in Table 2, show that, as may be expected, the only significant contributions are those corresponding to height symmetric functions in the x-direction and one S.S. beam function in the y-direction. A second calculation was made with 8 symmetric plate functions corresponding to $m = 8$ symmetric CC beam functions in the x-direction and one S.S. beam function in the y-direction($n = 1$). The numerical results presented in Table 3 prove that neglecting the antisymmetric modes leads to the same results listed in Table 2.

3.2 Numerical Validation

A computer program performed for this work using MATLAB software calculates the linear frequency parameters expressed in Equation 21 and plots the normalized mode shape defined in Equation 2. To verify the validity and precision of the present analysis, the three-span rectangular plate displayed in Figure 1 is examined for two plates with three boundary conditions SSSS, CSSS and CCSS. The first plate, noted plate (1), has an aspect ratio $\alpha = 4$ and the two intermediate lines located at $x_1 = 0.25$ and $x_2 = 0.75$. The second plate, noted plate (2), has an aspect ratio $\alpha = 3$, and the two intermediate lines located at $x_1 = 1/3$ and $x_2 = 2/3$. Table 4 lists the first six frequency parameters $\Omega_k = \omega_k.\left(\frac{a}{\alpha}\right)^2\sqrt{\rho.H/D}$ for the two plates. For uniformity of computation, the symmetric and asymmetric modes were used in the x-direction, which leads to the use of 16 trial beam functions in this direction and two beam functions in the y-direction. The results of plate (1) are compared to those found using the Rayleigh-Ritz method and given by Zhou, [15] Kim, [8] Liew [11] and Mizusawa [9]; it also compared to the resultants given by Wu [10] using the finite strip method. The most accurate results in Table 4 are those found by Zhou [16], thanks to its small values. Zhou [16] has developed static solutions of a point-supported beam under a series of sine loads as a set of admissible functions. The comparison with these latter results shows that (1) some present results are smaller than that of Ref [16]. (2) the difference percentages remain less than 0.67% for the six frequency parameters and the three boundary conditions considered.

Table 2. The contribution coefficient $a_k = a_{ij}$ of the first ten modes of the continuous CCSS plate type (a), $\alpha = 4$. $m = 16$, $n = 2$

i	j	Mode 1	Mode 2	Mode 3	Mode 4	Mode 5	Mode 6	Mode 7	Mode 8	Mode 9	Mode
1	1	8,70E-	3,16E-	-2,03E-	1,03E-	-2,46E-	-8,51E-	7,31E-	1,68E-03	-1,62E-	-3,48E-
2	1	-4,35E-	4,54E-	5,71E-	5,90E-	-1,27E-	7,04E-	2,63E-	1,66E-01	-1,63E-	-5,39E-
3	1	-4,91E-	3,74E-	-4,34E-	1,67E-	-4,55E-	4,19E-	1,43E-	1,74E-03	-3,78E-	-6,82E-
4	1	-9,55E-	-8,87E-	2,44E-	3,67E-	-9,97E-	1,35E-	-6,93E-	6,58E-02	-7,07E-	-3,07E-
5	1	3,38E-	7,97E-	-8,49E-	9,63E-	4,58E-	-3,11E-	1,83E-	-1,36E-04	-5,22E-	-1,43E-
6	1	-1,34E-	7,88E-	6,61E-	7,03E-	-3,27E-	4,90E-	1,77E-	-3,12E-01	6,15E-	-2,57E-
7	1	3,27E-	2,28E-	-1,97E-	4,01E-	-7,17E-	-9,14E-	-2,48E-	2,69E-02	-2,70E-	-6,57E-
8	1	-6,80E-	5,76E-	1,35E-	9,60E-	9,26E-	2,19E-	-2,39E-	9,24E-01	-1,41E-	-6,63E-
9	1	-7,40E-	2,32E-	-2,42E-	-5,00E-	2,95E-	6,94E-	2,07E-	-1,70E-03	2,02E-	1,81E-
10	1	-5,28E-	-2,00E-	3,58E-	-4,30E-	1,13E-	3,31E-	7,23E-	-7,36E-02	1,44E-	1,29E-
11	1	-7,05E-	-1,15E-	1,12E-	-7,32E-	4,68E-	7,51E-	3,07E-	-2,76E-02	4,80E-	2,81E-
12	1	-1,42E-	-5,78E-	1,51E-	1,09E-	2,24E-	4,17E-	-3,86E-	3,20E-02	-1,76E-	-2,48E-
13	1	3,79E-	5,82E-	-3,14E-	-2,46E-	-4,75E-	-8,31E-	1,67E-	-6,18E-02	4,23E-	6,15E-
14	1	-3,30E-	8,95E-	4,60E-	2,64E-	2,12E-	5,42E-	-1,37E-	6,61E-02	-8,86E-	-6,43E-
15	1	4,42E-	-1,63E-	-2,21E-	-1,65E-	-3,80E-	-7,22E-	1,08E-	-2,72E-02	1,19E-	3,33E-
16	1	-3,26E-	4,74E-	9,89E-	1,93E-	2,01E-	4,90E-	-9,58E-	3,14E-02	-3,29E-	-3,81E-
1	2	-8,33E-	-1,24E-	1,68E-	-7,06E-	2,01E-	-8,83E-	8,12E-	-3,52E-10	-2,07E-	-4,31E-
2	2	6,09E-	-3,44E-	-4,09E-	-4,26E-	7,67E-	8,58E-	4,60E-	-7,49E-11	1,53E-	-5,85E-
3	2	4,53E-	-2,10E-	3,18E-	-1,40E-	2,55E-	4,63E-	1,56E-	-8,45E-10	-5,05E-	-8,87E-
4	2	1,61E-	6,58E-	-1,79E-	-2,61E-	7,08E-	2,89E-	-8,84E-	-4,27E-10	5,55E-	-3,64E-
5	2	-3,30E-	-6,34E-	5,89E-	-6,57E-	-2,01E-	-4,50E-	2,57E-	-1,29E-09	-7,48E-	-2,11E-
6	2	-3,38E-	-5,43E-	-4,70E-	-4,89E-	2,08E-	3,03E-	6,59E-	-3,20E-11	1,60E-	-6,64E-
7	2	-3,72E-	-1,60E-	1,66E-	-6,15E-	4,03E-	-5,03E-	1,04E-	-4,92E-10	-2,84E-	-5,49E-
8	2	1,20E-	-8,74E-	-1,08E-	-8,74E-	-2,99E-	1,72E-	-2,44E-	-3,96E-10	4,08E-	-1,40E-
9	2	1,95E-	-3,37E-	2,33E-	-6,43E-	-1,97E-	1,96E-	2,68E-	-5,34E-12	-4,20E-	7,62E-
10	2	-1,36E-	2,41E-	-1,04E-	3,01E-	-6,74E-	1,54E-	-3,51E-	4,28E-11	3,02E-	3,53E-
11	2	1,24E-	2,21E-	-3,98E-	7,09E-	-3,04E-	1,29E-	-1,37E-	2,09E-11	4,82E-	1,63E-
12	2	2,46E-	6,17E-	-8,64E-	-9,84E-	-1,25E-	4,04E-	-1,03E-	1,22E-11	2,59E-	-2,16E-
13	2	-5,82E-	1,23E-	2,82E-	1,71E-	3,37E-	-9,11E-	2,97E-	-6,09E-11	-6,78E-	3,36E-
14	2	4,74E-	-9,58E-	-2,74E-	-2,82E-	-1,29E-	7,12E-	1,50E-	-2,76E-11	1,76E-	-4,75E-
15	2	-8,15E-	3,37E-	2,26E-	1,44E-	3,02E-	-1,08E-	-2,86E-	-5,10E-11	-4,83E-	2,30E-
16	2	5,31E-	-6,07E-	-6,62E-	-1,89E-	-1,40E-	6,86E-	8,25E-	0,00E+00	2,08E-	-3,07E-

Table 3. The contribution coefficient $a_k = a_{ij}$ of the modes of the continuous CCSS studied plate, $\alpha = 4$. $m = 8$, $n = 1$.

a_{ij}	Mode 1	Mode 2	Mode 3	Mode 4	Mode 5	Mode 6	Mode 7	Mode 8
a_{11}	8,68E-01	1,96E-01	-2,44E-01	1,80E-01	6,96E-02	-6,44E-02	1,70E-01	-2,80E-01
a_{21}	-4,95E-01	4,15E-01	-4,48E-01	2,98E-01	1,10E-01	-1,03E-01	2,70E-01	-4,45E-01
a_{31}	3,31E-02	8,67E-01	4,35E-01	-1,14E-01	-5,60E-02	3,87E-02	-1,04E-01	1,72E-01
a_{41}	3,22E-02	1,92E-01	-7,39E-01	-3,69E-01	-1,55E-01	9,95E-02	-2,57E-01	4,24E-01
a_{51}	-7,59E-04	2,37E-04	3,08E-03	-2,63E-02	6,08E-03	9,77E-01	1,13E-01	-1,76E-01
a_{61}	-7,87E-03	-1,38E-02	5,53E-02	-8,53E-01	6,99E-02	-1,30E-01	2,60E-01	-4,25E-01
a_{71}	1,43E-03	2,05E-02	-2,85E-02	-5,01E-02	9,75E-01	3,75E-02	-1,06E-01	1,80E-01
a_{81}	4,16E-05	2,06E-04	-2,91E-04	1,91E-03	-2,59E-03	-5,26E-03	8,54E-01	5,20E-01

The results of the plate (2) are also compared to those found using R.R.M. and given by Zhou, [14]; he chose a combination of beam eigenfunctions and polynomials as trial beam functions and 25 trial plate functions were considered in this reference.

It is noted that

1) the difference percentages remain less than 1.88%.

2) Actual results are the smallest in this Table, so they are the most accurate.

Table 4. First six frequency parameters, $\Omega_k = \omega_k . b^2\sqrt{\rho . H/D}$, of the three-span continuous rectangular plates, with three boundary conditions (B.C.).

B.C.		Ω_1	Ω_2	Ω_3	Ω_4	Ω_5	Ω_6
Plate (1) $\alpha = 4$, $x_1 = 1/4$ and $x_2 = 3/4$							
SSSS	Present	12.926	19.739	21.572	23.743	35.328	42.259
	Zhou [16]	12.919	19.739	21.534	23.647	35.215	42.245
	Azimi [7]	12.920	19.740	21.530	23.650	35.210	42.240
	Mizusawa	12.921	19.741	21.551	23.682	35.415	0.000
	Wu	12.920	19.740	21.550			
	Kim	12.930	19,739	21.594	23.812	35.401	42.268
	Liew	12.924	19.739	21.531	23.653	35.283	42.254
CSSS	Present	12.948	20.056	22.621	26.598	35.661	42.262
	Zhou [16]	12.938	20.097	22.643	26.506	35.605	42.247
	Azimi [7]	12.940	20.100	22.640	26.500	35.590	42.240
	Wu	12.940	20.100	22.670			
	Kim	12.972	20.118	22.916	26.915	36.628	42.307
	Liew	12.961	20.114	22.866	26.514	36.164	42.286
CCSS	Present	12.972	20.800	25.524	27.302	36.098	42.271
	Zhou [16]	12.957	20.816	25.648	27.128	35.980	42.249
	Azimi [7]	12.960	20.810	25.640	27.120	35.970	42.250
	Wu	12.960	20.830	25.690			
	Kim	12.967	20.828	25.684	27.262	36.170	42.296
	Liew	12.963	20.814	25.654	27.179	35.998	42.263
Plate (2) $\alpha = 3$, $x_1 = 1/3$ and $x_2 = 2/3$.							
SSSS	Present	19.719	21.443	26.805	49.250	49.317	50.383
	Zhou [14]	19.739	21.854	26.373	49.348	49.348	50.876
	Azimi [7]	19.74	21.6	26	49.35		
CSSS	Present	20.216	23.780	28.541	49.628	50.706	51.940
	Zhou [14]	20.269	23.843	28.523	49.712	50.848	52.029
	Azimi [7]	20.22		28.07	49.63	50.69	
CCSS	Present	21.868	25.777	29.476	50.735	53.106	54.996
	Zhou [14]	21.611	26.235	29.507	50.545	53.661	55.206

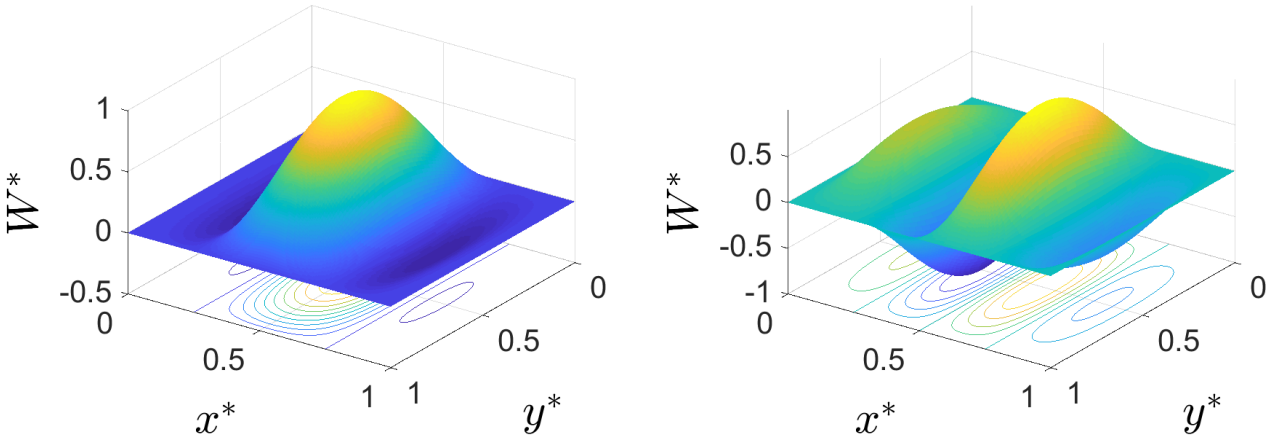

Fig. 4 The first and second modes of CCSS plate (1) for $\alpha = 4$.

The Matlab software code performed for this work is validated by plotting the first and the second mode of the CCSS studied plate for an aspect ratio $\alpha = 4$; the perspective drawings of these two modes are shown in Figure 4; both symmetric and asymmetric modes have been considered, 16 CC beam functions were used in the x-direction, and 2 S.S. beam functions were used in the y-direction. In addition to this, the normalized cross-sections of the four lowest normalized mode shapes at the plate middle $x^* = 0.5$ and $y^* = 0.5$ are depicted in Figure 5 and Figure 6 for an aspect ratio $\alpha = 4$ and $\alpha = 0.25$, respectively. The same curves are plotted in Figure 7 for plate (2). Figures 5 to 7 show that all four modes are zero at the intermediate lines, which leads to conclude that the hypothesis of modeling the support line by a distribution of translation springs is verified. It should be noted that Figs. (5) to (7) show that the slopes corresponding to clamped edges (at $x^* = 0$ and $x^* = 1$) are zero. On the other hand, Figure 5 shows that the cross-sections at $x^* = 0.5$ of the normalized four mode shapes are superposed. This is explained by the fact that the width b is small enough for an aspect ratio $\alpha = 4$. Figure 6 shows that the cross-sections in the x-direction of the first two mode shapes are superposed: the length a is too small since $\alpha = 0.25$. However, the crosse sections in the y-direction are no longer superposed. The cross-sections of the first and third normalized mode shapes are superposed, and those of the second and fourth normalized mode shapes are superposed.

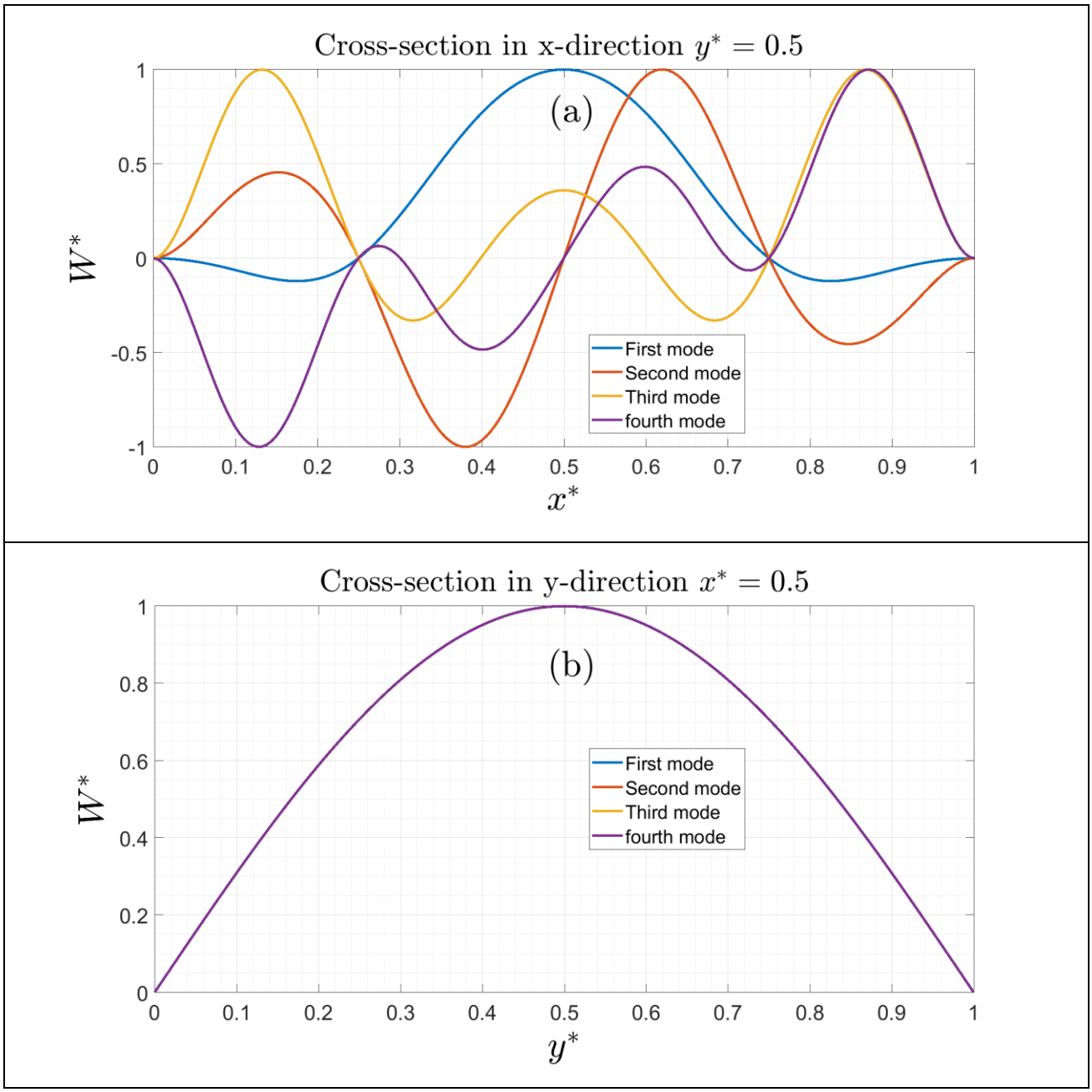

Fig. 5 Normalized cross-sections of the four lowest mode shapes at the middle of the CCSS plate (1) for $\alpha = 4$, in the x-direction $y^* = 0.5$, and in the y-direction $x^* = 0.5$

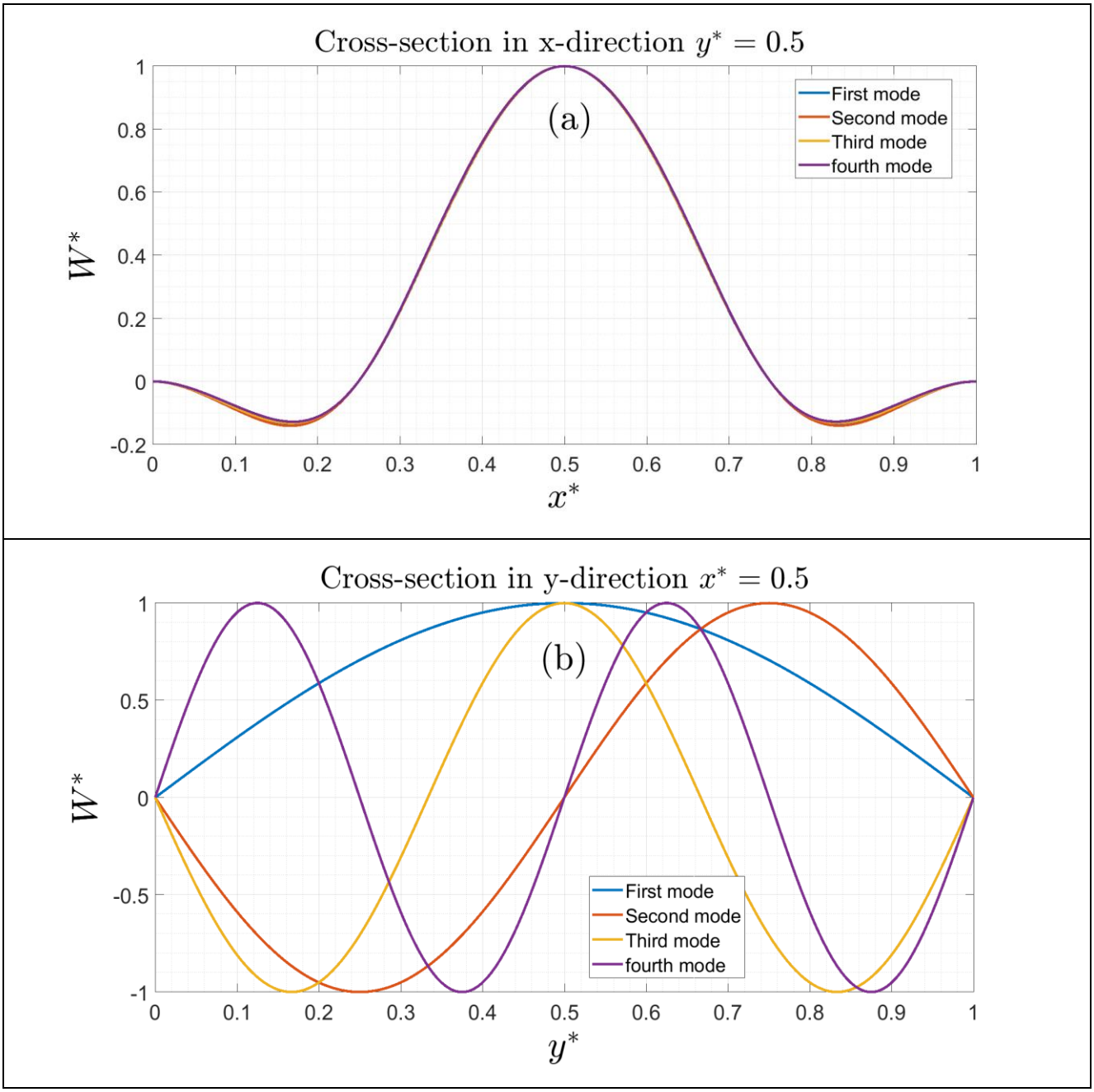

Fig. 6 Normalized cross-sections of the four lowest mode shapes at the middle of the CCSS plate (1) for $\alpha = 0.25$, in the x-direction $y^* = 0.5$, and in the y-direction $x^* = 0.5$

4. Nonlinear Vibrations of the Rectangular Plate Resting on Line Support

This section examines the difficult problem of the nonlinear vibration for the three-span continuous CCSS rectangular plates noted plate (1). Benamar's method was used in the present section to calculate the coefficient contribution vector {A} and of the nonlinear frequency parameters Ω in order to determine the fundamental nonlinear mode shape w_1.

Determination of the coefficient contribution vector and nonlinear frequency parameter

The nonlinear geometrical rigidity tensor [B{A}] is taken into account in Eqs (17), whose tensorial form is written as follows [34]:

$$2a_i k^*_{ir} + 3a_i a_j a_k b^*_{ijkr} - 2\Omega^2 a_i m^*_{ir} = 0 \quad r = 1..N \qquad (23)$$

This nonlinear system has N equations and $(N+1)$ unknowns, which are the N components of the contribution coefficient vector $\{a_1 \ a_2 \ \dots \ a_N\}$ and the nonlinear frequency parameter Ω denoted in what follows Ω_{NL}. Consequently, a further equation must be added to Eqs (23) to complete the formulation. The principle of conservation of energy allows giving the expression of Ω^2_{NL} [51]:

$$\Omega^2_{NL} = \frac{a_i a_j k_{ij} + a_i a_j a_k a_l b_{ijkl}}{a_i a_j m_{ij}} \qquad (24)$$

On the other hand, the first component a_1 of the unknown vector $\{A\}$ is assigned. Therefore, the index r written in Equation (23) varies from 2 to N.

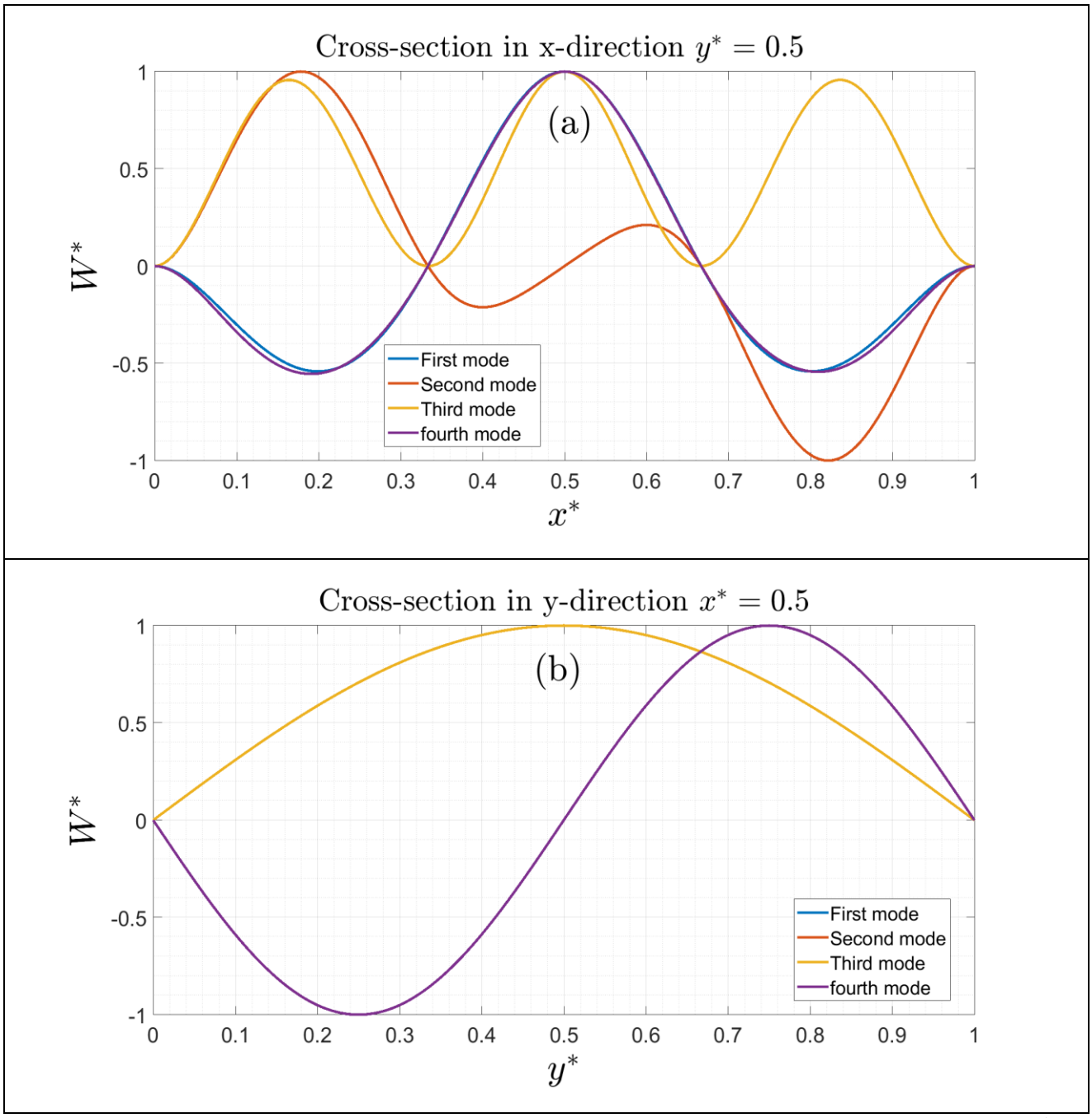

Fig. 7 Normalized cross-sections of the four lowest mode shapes at the middle of the CCSS plate (2) $\alpha = 3$, in the x-direction $y^* = 0.5$, and in the y-direction $x^* = 0.5$

By replacing the frequency parameter expression given in Equation (24) in Equation (23), one gets $(N-1)$ nonlinear equations to solve:

$$a_i k^*_{ir} + 1.5 a_i a_j a_k b^*_{ijkr} - \frac{a_i a_j k_{ij} + a_i a_j a_k a_l b_{ijkl}}{a_i a_j m_{ij}} a_j m^*_{ir} = 0 \quad (25)$$

$r = 2..N$. Approximate methods such as the single mode approach, the first and second formulation, are often used in the vibration investigation of beam, plate and shell [40-47]. These approximate methods give questionable results when the nonlinearity increases. In order to avoid using these approximate methods, a Matlab iterative code, performed for this work, allows for solving the nonlinear system expressed in Equation 25. The solution is based on the least squares method for the nonlinear system using the lsqnonlin routine from Matlab. This routine starts at a given initial solution estimate and finds a minimum sum of squares of the functions defined in Equation 25. The initial solution requested by the cited routine is given by the approximate method called the second formulation developed by Benamar-El Kadiri [18]. Once the contribution coefficient vector $\{a_1\ a_2\ \ldots a_N\}$ has been found, they are injected into Equation 25 in order to calculate (n-1) differences H_r as well as the residual is the sum of the squares of these differences noted $\mathfrak{Res}$. The differences H_r and the residuals $\mathfrak{Res}$ are defined by:

$$H_r = a_i k^*_{ir} + 1.5 a_i a_j a_k b^*_{ijkr} - \frac{a_i a_j k_{ij} + a_i a_j a_k a_l b_{ijkl}}{a_i a_j m_{ij}} a_j m^*_{ir}, \quad \Re es = \sum_{r=2}^{N} H_r^2 \tag{26}$$

The results are supposed to be validated when the residuals $\Re es$ remain less than 10^{-7}.

4.1. Amplitude Dependence of the Mode Shapes and the First Nonlinear Frequency

The contribution coefficient vector {A} are calculated by solving Equation (25) as well as the nonlinear frequency parameters Ω_{NL} by Equation (24) for an assigned first contribution a_1 of the first trial plate function w_1^*. On the other hand, the convergence study carried out above allowed to use of $m = 8$ symmetric modes in the CC direction and one mode in the S.S. direction ($n = 1$). From this consideration, the fundamental nonlinear mode expressed in Equation 2 is written in dimensionless form as:

$$w^*(x^*, y^*, a_1) = \sum_{k=1}^{8} a_{(2k-1)} w^*_{(2k-1)}(x^*, y^*) \tag{27}$$

The assigned a_1 is the first component of the contribution coefficient vector $\{A\} = \{a_1 \ \ a_3 \ \ a_5 \ \ \dots a_{13}\}^T$, it varies from 0.05 to 0.5 in the present work. Tables 4 and 5 summarize the result of the vector {A} for several values of a_1 for aspect ratios $\alpha = 4$ and 0.25, respectively. These contribution coefficients are included in expression 27 in order to calculate the fundamental nonlinear mode $w^*(x^*, y^*, a_1)$ whose maximum values, denoted W_{max}, are listed in the first column of the two Tables. In addition, Equation 24 calculates the fundamental nonlinear frequency parameters Ω_{NL} allowing getting the ratios $\frac{\Omega_{NL}}{\Omega}$, Ω being the linear frequency parameters. These ratios are listed in the second column of Tables 4 and 5. The residuals $\Re es$ calculated by Equation 26 are listed in the last column of the latter tables.

Table 5. W^*_{Max}. Ω_{NL}/Ω and a_k as function of a_1 for the CCSS studied plate for $\alpha = 4$

W^*_{Max}	Ω_{NL}/Ω	a_1	a_3	a_5	a_7	a_9	a_{11}	a_{13}	a_{15}	$\Re es$
1,70E-01	1,0152	0,0500	-0,03	1,72E-03	1,94E-03	-4,50E-05	-4,66E-04	9,12E-05	2,10E-06	3,03E-08
3,36E-01	1,0589	0,1000	-0,06	2,46E-03	4,37E-03	-9,55E-05	-1,01E-03	1,91E-04	4,81E-06	5,84E-11
4,97E-01	1,1263	0,1500	-0,08	1,47E-03	7,60E-03	-1,53E-04	-1,69E-03	3,00E-04	8,70E-06	5,38E-11
6,52E-01	1,2123	0,2000	-0,11	-1,63E-03	1,17E-02	-2,14E-04	-2,54E-03	4,06E-04	1,43E-05	1,15E-08
8,02E-01	1,3123	0,2500	-0,14	-7,00E-03	1,64E-02	-2,73E-04	-3,58E-03	4,92E-04	2,20E-05	3,92E-10
1,00E+00	1,4647	0,3180	-0,18	-1,80E-02	2,32E-02	-3,44E-04	-5,28E-03	5,44E-04	3,62E-05	1,00E-08
1,09E+00	1,5416	0,3500	-0,20	-2,47E-02	2,63E-02	-3,75E-04	-6,17E-03	5,36E-04	4,44E-05	1,83E-12
1,23E+00	1,6672	0,4000	-0,23	-3,72E-02	3,08E-02	-4,27E-04	-7,64E-03	4,79E-04	5,89E-05	1,07E-10
1,38E+00	1,7986	0,4500	-0,26	-5,26E-02	3,42E-02	-4,97E-04	-9,17E-03	3,83E-04	7,52E-05	1,78E-09
1,52E+00	1,9349	0,5000	-0,30	-7,11E-02	3,64E-02	-6,11E-04	-1,07E-02	2,79E-04	9,29E-05	6,08E-11

Table 6. W^*_{Max}. Ω_{NL}/Ω and a_k as function of a_1 for the CCSS studied plate for $\alpha = 0.25$

W^*_{Max}	Ω_{NL}/Ω	a_1	a_3	a_5	a_7	a_9	a_{11}	a_{13}	a_{15}	$\Re es$
0,1729	1,0077	0,05	-2,98E-02	1,39E-03	9,70E-04	-1,14E-05	-1,68E-04	3,77E-05	-4,15E-08	4,10E-09
0,3111	1,0246	0,09	-5,37E-02	2,46E-03	1,74E-03	-1,84E-05	-3,19E-04	6,70E-05	3,49E-08	8,55E-11
0,5185	1,0669	0,15	-8,96E-02	3,93E-03	2,88E-03	-2,20E-05	-6,00E-04	1,08E-04	5,23E-07	2,16E-09
0,7016	1,1193	0,20	-1,21E-01	5,07E-03	3,85E-03	-1,48E-05	-9,26E-04	1,37E-04	1,51E-06	5,24E-09
0,8744	1,1797	0,25	-1,51E-01	5,98E-03	4,71E-03	3,42E-06	-1,32E-03	1,58E-04	3,07E-06	9,49E-10
1,0023	1,2304	0,29	-1,73E-01	6,56E-03	5,31E-03	2,51E-05	-1,67E-03	1,68E-04	4,68E-06	3,78E-12
1,0369	1,2448	0,30	-1,79E-01	6,70E-03	5,46E-03	3,22E-05	-1,77E-03	1,70E-04	5,19E-06	3,06E-11
1,2100	1,3214	0,35	-2,09E-01	7,35E-03	6,17E-03	7,66E-05	-2,36E-03	1,71E-04	8,24E-06	2,58E-12
1,3939	1,4094	0,40	-2,41E-01	7,91E-03	6,80E-03	1,40E-04	-3,10E-03	1,59E-04	1,24E-05	1,25E-11
1,5572	1,4922	0,45	-2,70E-01	8,33E-03	7,25E-03	2,11E-04	-3,86E-03	1,37E-04	1,70E-05	2,38E-10
1,7315	1,5843	0,50	-3,00E-01	8,71E-03	7,61E-03	3,01E-04	-4,78E-03	9,94E-05	2,27E-05	1,08E-11

From Tables 5 and 6, some observations must be emphasised: (1) the residuals $\mathfrak{Res}$, listed in the last column, are very low and do not exceed 4.11×10^{-9} for the whole range of the assigned a_1 considered. One can conclude that the calculations of the nonlinear system expressed in Equation 17 are accurate. (2) The contribution coefficient of the modes decreases as the index i in a_i increases. (3) the rate of increase in the fundamental nonlinear frequency Ω_{NL} with increasing the dimensionless maximum deflection W^*_{Max} is quite low at small amplitudes. It can be concluded that the linear frequency parameters can be used for low amplitudes with accepted accuracy. However, the effect of nonlinearity is very acute when the amplitudes reach approximately once the thickness of the plate. In effect, the increase in the nonlinear fundamental frequency parameters with respect to the first linear frequency is about 23% and 46% in cases $\alpha = 0.25$ and $\alpha = 4$, respectively, for vibration amplitudes equal to plate thickness H.

4.2. Backbone curves

In vibration studies of the classical plates without intermediate lines, the hardening effect is monotonic to the aspect ratio α. The present section deals with the variation of the hardening effect on the continuous CCSS studied plate as a function of α. The Matlab software code cited above calculated the dimensionless maximum deflection W^*_{Max} and the ratio $\frac{\Omega_{NL}}{\Omega}$ for different values of the aspect ratio of the range $[0.24, 4]$ for the value of the contribution coefficient of the first mode $a_1 = 0.5$. The results are summarized in Table 7, and their accuracies are validated by the residuals listed in the last line.

Figure 9 plots two curves $W^*_{Max} = f(\alpha)$ and $\frac{\Omega_{NL}}{\Omega} = f(\alpha)$. Table 7 and Figure 9 shows that W^*_{Max} is strictly decreasing as a function of the aspect ratio α. However, the ratio Ω_{NL}/Ω is decreasing up to about $\alpha = 1.04$, after what it increases. One can conclude that the curves $W^*_{Max} = f\left(\frac{\Omega_{NL}}{\Omega}\right)$, denoted backbone curves, change his behavior at the value of the aspect ratio $\alpha = 1.04$. This result was illustrated in Figure 10: the hardening type decrease very slightly when $\alpha < 1.04$. However, for an aspect ratio greater than 1.04, the hardening increases.

Table 7. W^*_{Max} and $\frac{\Omega_{NL}}{\Omega}$ as a function of α for the CCSS studied plate for $a_1 = 0.5$

α	0,24	0,44	0,64	0,84	1,04	1,24	1,5	2,04	2,44	2,84	3	4
W^*_{Max}	1,7315	1,7305	1,7288	1,7263	1,7228	1,7181	1,7099	1,6839	1,6562	1,6224	1,6077	1,5190
Ω_{NL}/Ω	1,5846	1,5775	1,5687	1,5608	1,5568	1,5592	1,5741	1,6449	1,7158	1,7861	1,8120	1,9349
$\mathfrak{Res}$	3,00E-10	1,09E-10	4,4E-09	5,6E-10	4,3E-12	8,88E-12	3,74E-12	1,79E-10	2,08E-11	8,24E-12	6,94E-08	7,12E-12

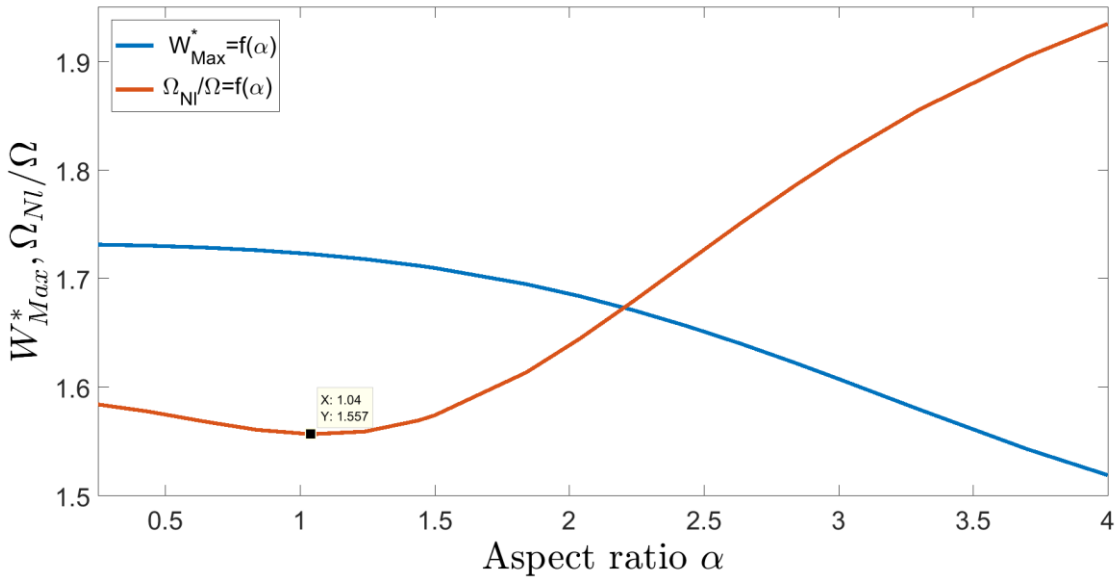

Fig. 8 Backbone curves of the CCSS plate type (a) in the vicinity of the first mode for various values of the aspect ratio α.

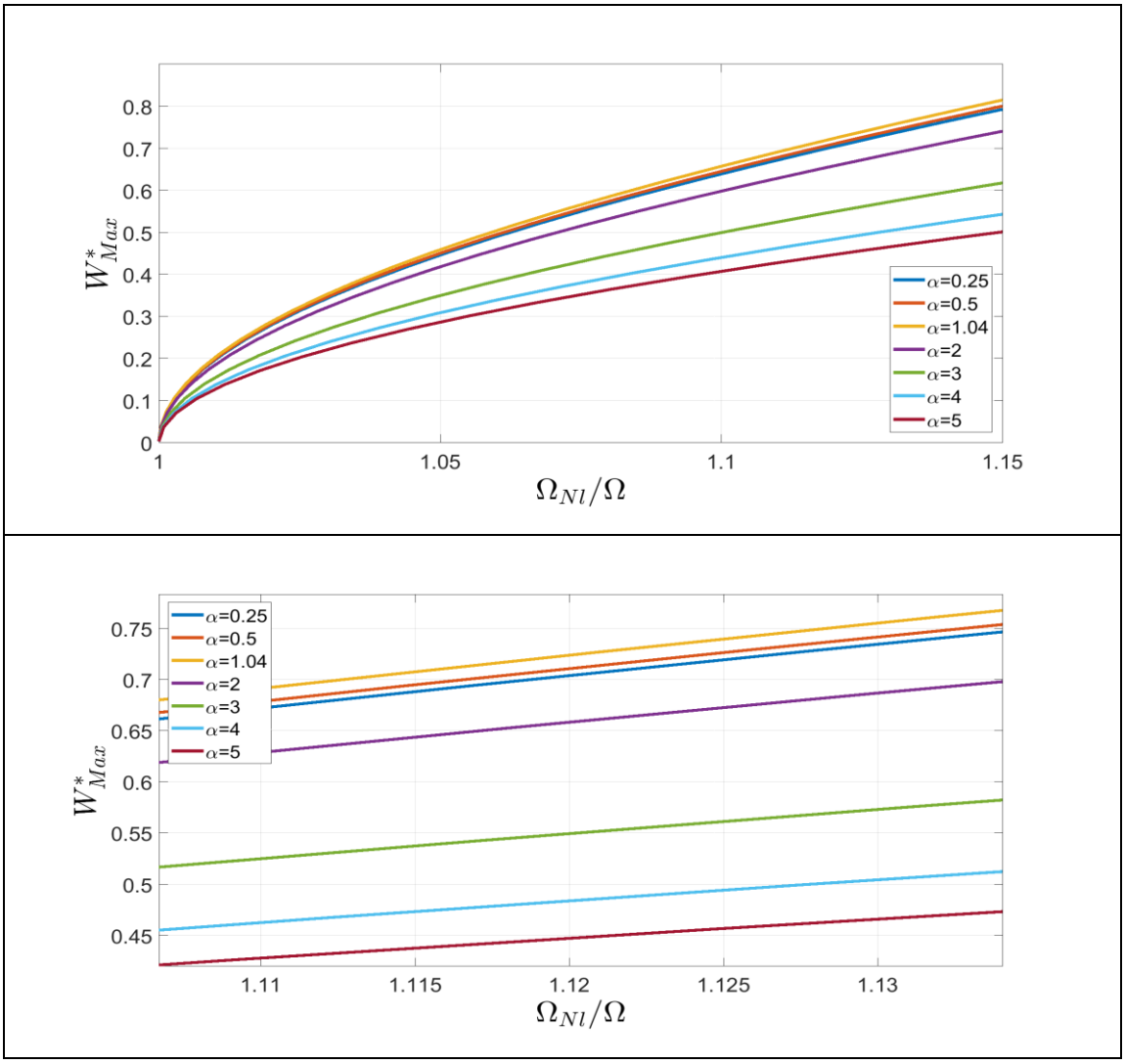

Fig. 9 Backbone curves of the CCSS plate type (a) in the vicinity of the first mode for various values of the aspect ratio α.

4.3. The Fundamental Nonlinear Mode

The fundamental nonlinear mode of the studied plate is determined by Equation 27 and plotted in Figure 6; m=8 symmetrical CC and one S.S. trial beam functions were used in the x and y-direction, respectively the aspect ratio is $\alpha = 4$ and the first component of the vector contribution $a_1 = 0.5$. The four lowest normalized cross-sections of the amplitude-dependent nonlinear fundamental mode for increasing the values of a_1, at the middle plate lines $y^* = 0.5$ and $x^* = 0.5$, are given in Figs (7) and (8) for aspect ratios $\alpha = 4$ and $\alpha = 0.25$, respectively. All curves depicted in these latter Figures show that: (1) From Figure 7, it is noticed that the amplitude dependence of the mode shapes is accentuated for $\alpha = 4$, but Figure 8 shows that this dependence is low for aspect ratios $\alpha = 0.25$; this result agrees very well with the above conclusion concerning the backbone curve when the plate aspect ratio verify $\alpha \leq 1.04$. It should be remembered that, for the studied plate, the length of the intermediate lines increases when the aspect ratio decreases. One can conclude that in the presence of the intermediate lines, and for $\alpha \leq 1.04$, the effect of the amplitude on the mode shapes is low. (2) The curvatures near the clamped edges increase with the dimensionless maximum deflection W_{Max}. (3) The mode does not change shape in the y-direction when incrementing the amplitude, thanks to the unique S.S. beam function used in this direction. (4) As might be expected, all modes are null at the line supports located at $x_1^* = 0.25$ and $x_2^* = 0.75$, i.e., at the intermediate lines.

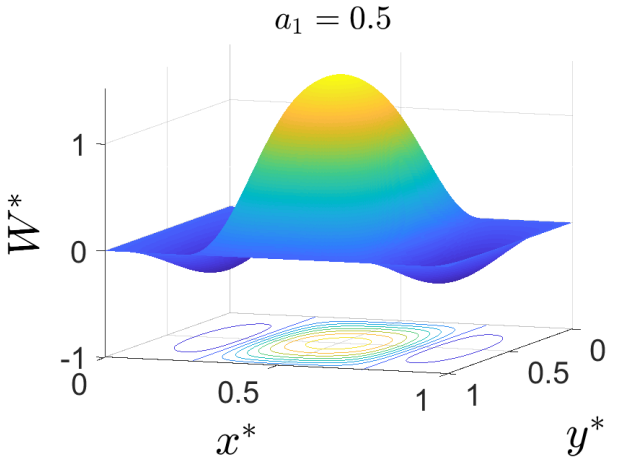

Fig. 10 The first normalized nonlinear mode shape of the CCSS studied plate for an aspect ratio α = 4.

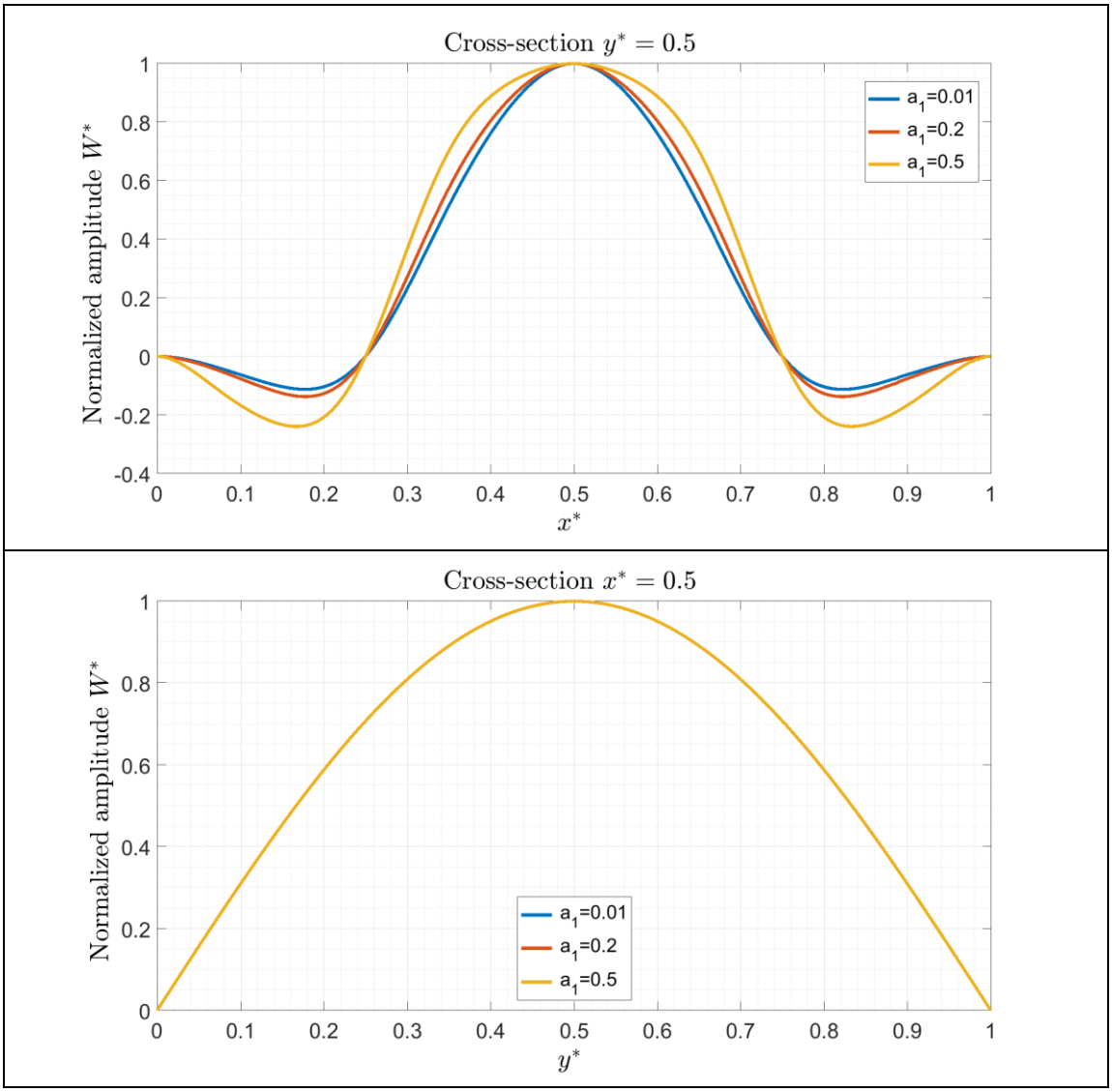

Fig. 11 (a) Normalized cross-sections in the x-direction $y^* = 0.5$, (b) Normalized cross-sections in the y-direction $x^* = 0.5$ of the first nonlinear mode shape of the CCSS three-span plate, $\alpha = 4$.

5. Nonlinear Forced vibrations

The purpose of this section is to examine the geometrically nonlinear forced vibrations of the CCSS studied plate for two values of the aspect ratio α. The harmonic excitation is the either concentrated force $F^c(x,y,t)$ applied at a known point (x_0,y_0), or to a distributed uniform force $F^d(x,y,t)$ applied to the entire plate area. The excitations F^c and F^d are modeled as follows:

$$\begin{aligned} F^c(x,y,t) &= F^c\delta(x-x_0)(y-y_0)\sin(\omega t) \\ F^d(x,y,t) &= F^d\sin(\omega t) \end{aligned} \quad (28)$$

in which δ is the Dirac function. Taking into account Equation (2), the generalized concentrated $F_i^c(t)$ and distributed $F_i^d(t)$ forces are deduced as follows:

$$\begin{aligned} F^c(x,y,t) &= F^c w_i(x_0,y_0) \quad \sin(\omega t) = f_i^c\sin(\omega t) \\ F^d(x,y,t) &= F^d\int_S w_i(x,y)dxdy \quad \sin(\omega t) = f_i^d\sin(\omega t) \end{aligned} \quad (29)$$

The dimensionless generalized forcing vector $\{f^*\}$ is defined by the expression:

$$\{f^*\} = \begin{cases} f_i^{*c} = \frac{a^3F^c}{bDH}w_i^*(x_0^*,y_0^*) \\ \quad in\ case\ of\ the\ concentrated\ force \\ f_i^{*d} = \frac{a^4F^d}{DH}\int_{S^*} w_i^*(x^*,y^*)dx^*dy^* \\ in\ case\ of\ the\ uniformly\ distributed\ force \end{cases} \quad (30)$$

where S^* is the dimensionless surface over what the uniformly distributed force F^d acts. The amplitude equation expressed by Equation 17 becomes in the nonlinear forced regime and using the matrix and tonsorial forms [18]:

$$\begin{aligned} &\left([K^*] - \Omega_{NL}^2[M^*]\right)\{A\} + 1.5[B^*\{A\}]\{A\} = \{f^*\} \\ &a_i k_{ir}^* + 1.5a_i a_j a_k b_{ijkr}^* - \Omega_{NL}^2 a_i m_{ir}^* = f_r^* \quad r = 1..N \end{aligned} \quad (31)$$

In the event of forced mode, Ω_{NL} It is no longer the unknown resonant frequency but the parameter of the known excitation frequency. It varies within a range according to excitation tests. The nonlinear algebraic system 31 has N equations and N unknowns which are the components of the contribution coefficient vector $\{A\}$.

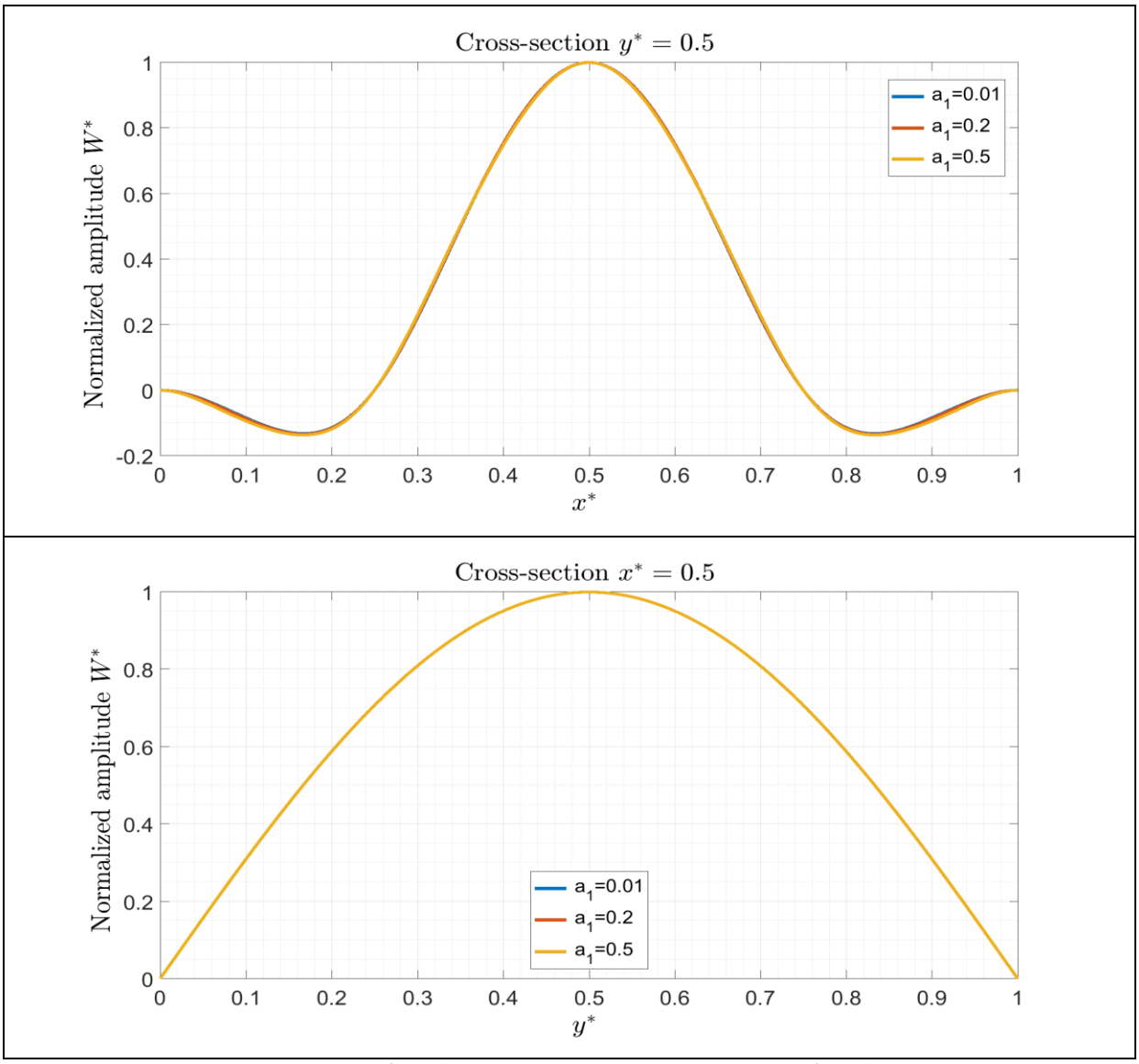

Fig. 12 (a) Normalized cross-sections in the x-direction $y^* = 0.5$, (b) Normalized cross-sections in the y-direction $x^* = 0.5$, of the first nonlinear mode shape of the CCSS three-span plate, $\alpha = 0.25$

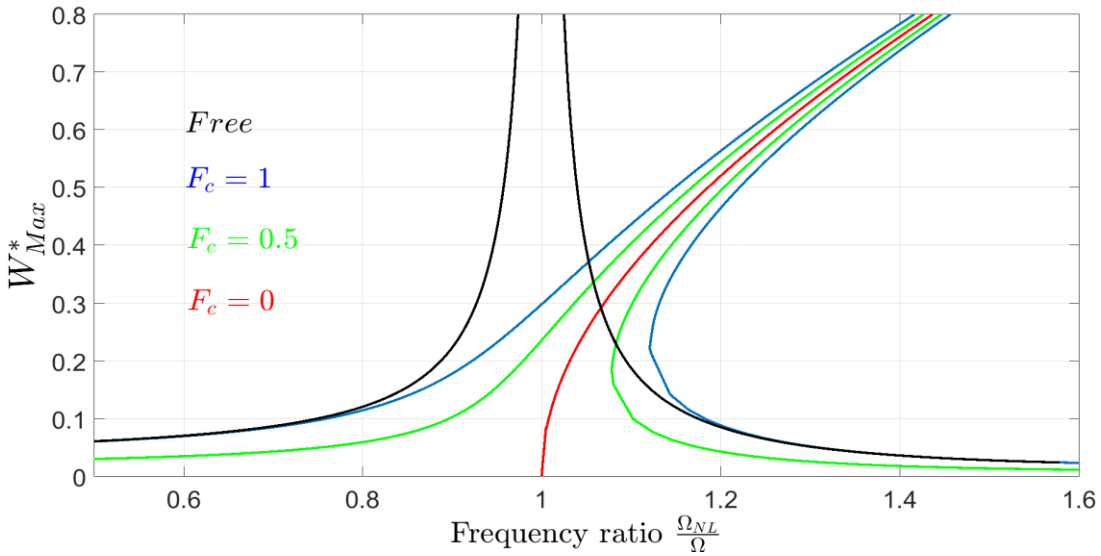

Fig. 13 Forced response of the CCSS studied plate excited by different levels of concentrated force $F_c = 0, 0.5, 1$ using the multi-mode approach in the vicinity of the fundamental mode for two aspect ratios($\alpha = 4$). Dashed curve: linear case, continuous curves: nonlinear case.

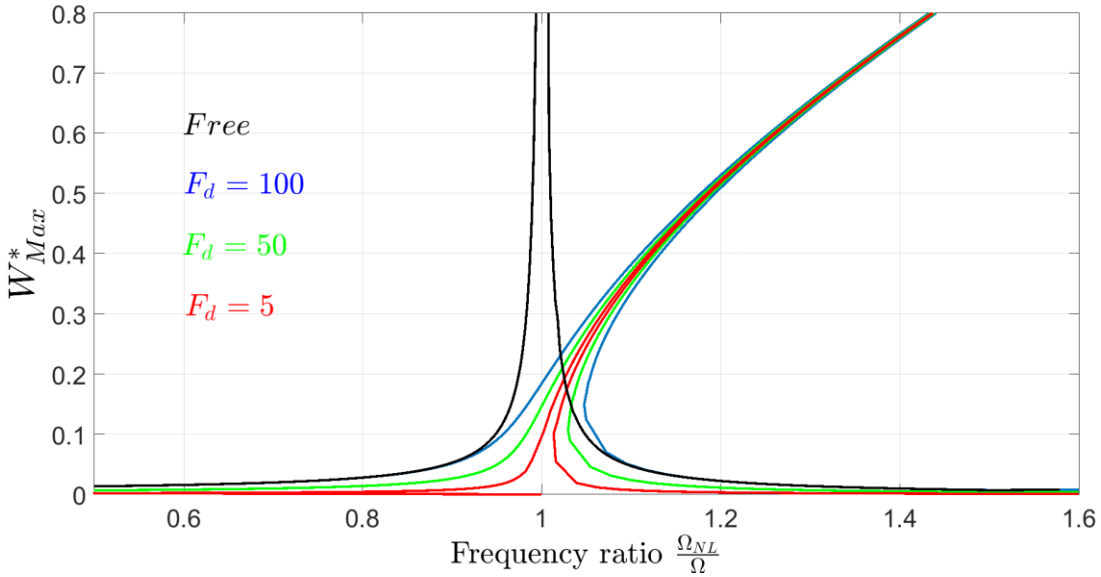

Fig. 14 Forced response of the CCSSS studied plate excited by different levels of distributed force using the multi-mode approach in the vicinity of the fundamental mode for two aspect ratios($\alpha = 4$). Dashed curve: linear case, continuous curves: nonlinear case.

A Matlab code, realized for the preset work and using the lsqnonlin routine, allows solving Equation 31 in order to obtain the N contribution coefficients $(a_1\ a_2 \ldots a_N)$. Then, these latter are injected into Equation 27 to calculate the nonlinear fundamental mode. The determination of the maximum value of the dimensionless deflection W^*_{Max} is then immediate. In what follows, one take $a = 0.24$, $b = a/\alpha$, $H = 0.0005$, $\rho = 7850$, and $E = 198 \times 10^9$.

The forced nonlinear dynamic behavior is investigated for the studied plate, which is excited by a concentrated force at the plate center $(x^* = 0.5, y^* = 0.5)$ and by a distributed force for aspect ratios $\alpha = 1{,}4$ and for different excitation levels. Figure 10 displays the linear and nonlinear forced frequency response function (NFFRF) in the vicinity of the fundamental mode in cases of concentrated for three excitation level $F_c = 0, 0.5{,}1$. The bashed black line plots the linear forced frequency response function. For excitation level $F_c = 0$ NFFRF coincides with the backbone curve corresponding to $\alpha = 4$ in Figure 13 (sky blue curve). Figure 14 shows the same curves for a distributed excitation. From these Figures, one can show that:

(1) a comparison between the linear and nonlinear frequency response functions when the continuous plate is excited by the same excitation level. The jump phenomenon commonly encountered in vibratory systems is observed. It is accentuated for the linear case.

(2) The comparison between the NFFRF of the studied plate, excited by different levels of concentrated forces $F_c = 0{,}0.5{,}1$ and of distributed forces $F_d = 5{,}50{,}100$ allows emphasis on the effect of geometrical nonlinearity with the multivalued region.

(3) The increase in the intensity of the excitation force is disproportionate to the increase in the amplitude of the NFFRF.

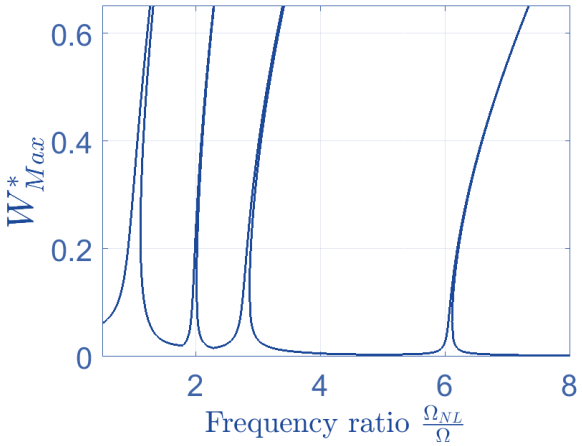

Fig. 15 Forced response of the CCSS continuous studied plate subjected to concentrated harmonic force $F_c = 1$ using the multi-mode approach up to the fourth resonant mode, with $\alpha = 4$

Figure (15) plots the NFFRF for a concentrated excitation at the plate center. The assigned nonlinear frequency Ω_{NL} varies up the fourth symmetric mode. The jump phenomenon that occurred at the resonance frequencies is well observed in the vicinity of the nonlinear frequencies, verifying $\frac{\Omega_{NL}}{\Omega_1} = 1.0,\ 1.979,\ 2.797,\ 6.095$ i, e when the frequency parameter of excitation Ω_{NL} becomes equal to the four linear frequency parameters $\Omega_1 = 12{,}978$, $\Omega_3 = 25{,}676$, $\Omega_5 = 36{,}292$, and $\Omega_7 = 79{,}075$, defined in Equation 21.

6. Conclusion

Linear and geometrically nonlinear free and forced vibrations of three-span rectangular plates have been studied by a new formulation of the Rayleigh-Ritz method. The line supports are modeled by distributions of elastic springs participating to the strain energy with a stiffness tending to infinity at the limit case of rigid supports. The trial plate functions are obtained as products of beam functions in the

x-and y-direction respecting the plate boundary conditions. They have been determined without taking into account the intermediate lines. The trial plate functions can be solved easily and unified independently of the line supports. Kinetic energy, linear strain energy due to the bending, nonlinear strain energy induced by the large vibration amplitudes and elastic strain energy stored in the spring distributions that model the line supports have been calculated and discretized. Afterwards, the application of Hamilton's principle allowed getting the classical nonlinear algebraic system governing the studied plate motion. An accurate convergence study has been carried out for the linear case. An investigation of the mode contribution coefficients reinforced this study's convergence. To validate the proposed solution, the linear vibrations of plates with different boundary conditions have been solved and compared to previously published results given by many authors showing a very good accuracy which leads to validate the present approach. The mode shapes and their cross-sections plotted showed that the deflections are zero at the line supports. In the linear vibrations, it is interesting to report that the intermediate lines inside the plate increase the frequency parameters.

Geometrically nonlinear free and forced vibrations have been examined by Benamar's method, using an iterative solution. The multi-mode approach was adopted without approximate methods. The amplitude-dependent fundamental modes are plotted. The aspect ratio influences the dependence of the mode on the amplitude; for the studied plate, it is more accentuated when the aspect ratio increases. The backbone curves have been plotted in order to investigate the hardening type. In this study, the hardening type is not a monotonic function of the aspect ratio. The forced vibrations were also analyzed. The effect of the excitation level on the plate dynamic behavior was illustrated and discussed. Moreover, a comparison of the linear and nonlinear frequency response was carried out. Concentrated and distributed excitations over the whole plate were utilized.

References

[1] A.S. Veletsos, and N.M. Newmark, "Determination of Natural Frequencies of Continuous Plates Hinged Along two Opposite Edges," Journal of Applied Mechanics, vol. 23, no. 1, pp. 97–102, 1956. [CrossRef] [Google Scholar] [Publisher Link]

[2] Eric E. Ungar, "Free Oscillations of Edge-connected Simply Supported Plate Systems," Journal of Manufacturing Science and Engineering, vol. 83, no. 4, pp. 434-439, 1961. [CrossRef] [Google Scholar] [Publisher Link]

[3] V.V. Bolotin, "A Generalization of the Asymptotic Method of the Eigenvalue Problems for Rectangular Regions," Inzhenernyi Zhurnal, vol. 3, pp. 86–92, 1961. [Google Scholar]

[4] Chien De-Lin V. N. Moskalenko, "On the Natural Vibrations of Multispan Plates," Prikladnaya Makhanika (in Russian), vol. 1, pp. 59–66, 1965.

[5] You-Kai Cheung, and Mo Shing Cheung, "Flexural Vibrations of Rectangular and Other Polygonal Plates," Journal of the Engineering Mechanics Division, vol. 97, no. 2, 1971. [CrossRef] [Google Scholar] [Publisher Link]

[6] Isaac Elishakoff, and Alexander Sternberg, "Eigenfrequencies of Continuous Plates with Arbitrary Number of Equal Spans," Journal of Applied Mechanics, vol. 46, no. 3, pp. 656–662, 1979. [CrossRef] [Google Scholar] [Publisher Link]

[7] S. Azimi, J.F. Hamilton, and W. Soedel, "The Receptance Method Applied to the Free Vibration of Continuous Rectangular Plates," Journal of Sound and Vibration, vol. 93, no. 1, pp. 9–29, 1984. [CrossRef] [Google Scholar] [Publisher Link]

[8] C.S. Kim, and S.M. Dickinson, "The Flexural Vibration of line Supported Rectangular Plate Systems," Journal of Sound and Vibration, vol. 114, no. 1, pp. 129–142, 1987. [CrossRef] [Google Scholar] [Publisher Link]

[9] T. Mizusawa, and T. Kajita, "Vibration of Continuous Skew Plates," Earthquake Engineering & Structural Dynamics, vol. 12, no. 6, pp. 847–850, 1984. [CrossRef] [Publisher Link]

[10] C.I. Wu, and Y.K. Cheung, "Frequency Analysis of Rectangular Plates Continuous in One or Two Directions," Earthquake Engineering & Structural Dynamics, vol. 3, no 1, pp. 1–14, 1974. [CrossRef] [Google Scholar] [Publisher Link]

[11] K.M. Liew, and K.Y. Lam, "Vibration Analysis of Multi-span Plates Having Orthogonal Straight Edges," Journal of Sound and Vibration, vol. 147, no. 2, pp. 255–264, 1991. [CrossRef] [Google Scholar] [Publisher Link]

[12] J. Kong, and Y.K. Cheung, "Vibration of Shear-deformable Plates with Intermediate Line Supports: A Finite Layer Approach," Journal of Sound and Vibration, vol. 184, no. 4, pp. 639–649, 1995. [CrossRef] [Google Scholar] [Publisher Link]

[13] Y.K. Cheung, and J. Kong, "The Application of a New Finite Strip to the Free Vibration of Rectangular Plates of Varying Complexity," Journal of Sound and Vibration, vol. 181, no. 2, pp. 341–353, 1995. [CrossRef] [Google Scholar] [Publisher Link]

[14] Ding Zhou, "Natural Frequencies of Elastically Restrained Rectangular Plates using a Set of Static Beam Functions in the Rayleigh-Ritz Method," Computers & Structures, vol. 57, no. 4, pp. 731–735, 1995. [CrossRef] [Google Scholar] [Publisher Link]

[15] D. Zhou, and Y.K. Cheung, "Free Vibration of Line Supported Rectangular Plates using a Set of Static Beam Functions," Journal of Sound and Vibration, vol. 223, no. 2, pp. 231–245, 1999. [CrossRef] [Google Scholar] [Publisher Link]

[16] D. Zhou, "Vibrations of Point-supported Rectangular Plates with Variable Thickness using a Set of Static Tapered beam Functions," International Journal of Mechanical Sciences, vol. 44, no. 1, pp. 149–164, 2002. [CrossRef] [Google Scholar] [Publisher Link]

[17] O.M. Ibearugbulem et al., "Simple and Exact Approach to Post Buckling Analysis of Rectangular Plate," SSRG International Journal of Civil Engineering, vol. 7, no. 6, pp. 54-64, 2020.[CrossRef] [Google Scholar] [Publisher Link]

[18] Yang Xiang, Y.B. Zhao, and G.W. Wei, "Discrete Singular Convolution and Its Application to the Analysis of Plates with Internal Supports. Part 2: Applications," International Journal for Numerical Methods in Engineering, vol. 55, no. 8, pp. 947–971, 2002. [CrossRef] [Google Scholar] [Publisher Link]

[19] C.F. Lü, Z.C. Zhang, and W.Q. Chen, "Free Vibration of Generally Supported Rectangular Kirchhoff Plates: State-Space-based Differential Quadrature Method," International Journal for Numerical Methods in Engineering, vol. 70, no. 12, pp. 1430–1450, 2007. [CrossRef] [Google Scholar] [Publisher Link]

[20] Abdelouahab Rezaiguia, and Debra F. Laefer, "Semi-analytical Determination of Natural Frequencies and Mode Shapes of Multi-span Bridge Decks," Journal of Sound and Vibration, vol. 328, no. 3, pp. 291–300, 2009. [CrossRef] [Google Scholar] [Publisher Link]
[21] Abdelouahab Rezaiguia et al., "Extension of Semi-analytical Approach to Determine Natural Frequencies and Mode Shapes of Multi-span Orthotropic Bridge Deck," Structural Engineering and Mechanics, vol. 43, no. 1, pp. 71–87, 2012. [CrossRef] [Google Scholar] [Publisher Link]
[22] M. Huang et al., "Free Vibration Analysis of Continuous Rectangular Plates," Journal of Sound and Vibration, vol. 329, no. 4, pp. 485–496, 2010. [CrossRef] [Google Scholar] [Publisher Link]
[23] Umut Topal, "Frequency Optimization of Laminated Composite Plates with Different Intermediate Line Supports," Science and Engineering of Composite Materials, vol. 19, no. 3, pp. 295–306, 2012. [CrossRef] [Google Scholar] [Publisher Link]
[24] Tiangui Ye et al., "A Modified Fourier Solution for Vibration Analysis of Moderately Thick Laminated Plates with General Boundary Restraints and Internal Line Supports," International Journal of Mechanical Sciences, vol. 80, pp. 29–46, 2014. [CrossRef] [Google Scholar] [Publisher Link]
[25] Md Arshad Jamal et al., "Rectangular Base Plate Design For Supporting Angular Member," SSRG International Journal of Civil Engineering, vol. 6, no. 7, pp. 13-16, 2019. [CrossRef] [Google Scholar] [Publisher Link]
[26] Youcef Fisli et al., "Dynamic Response of a Multi-span, Orthotropic Bridge Deck Under Moving Truck Loading with Tandem Axles," Diagnostyka, vol. 20, no. 4, pp. 37-48, 2019. [CrossRef] [Google Scholar] [Publisher Link]
[27] Farah Imed et al., "Free Vibration Analysis of Multi-span Orthotropic Bridge Deck with Rubber Bearings," Diagnostyka, vol. 22, no. 1, pp. 11-21, 2021. [CrossRef] [Google Scholar] [Publisher Link]
[28] Ignatius C. Onyechere et al., "Application of Polynomial Deflection Expression in Free-Vibration Study of Thick Rectangular Plates," SSRG International Journal of Civil Engineering, vol. 7, no. 7, pp. 53-64, 2020. [CrossRef] [Google Scholar] [Publisher Link]
[29] El Bekkaye Merrimi, Khalid El Bikri, and Rhali Benamar, "Geometrically Non-linear Steady State Periodic Forced Response of a Clamped–clamped Beam with an Edge Open Crack," Comptes Rendus Mécanique, vol. 339, no. 11, pp. 727–742, 2011. [CrossRef] [Google Scholar] [Publisher Link]
[30] M. El Kadiri, R. Benamar, and R.G. White, "Improvement of the Semi-analytical Method, for Determining the Geometrically Non-linear Response of Thin Straight Structures. Part I: Application to Clamped–clamped and Simply Supported–clamped Beams," Journal of Sound and Vibration, vol. 249, no. 2, pp. 263–305, 2002. [CrossRef] [Google Scholar] [Publisher Link]
[31] M. El Kadiri, and R. Benamar, "Improvement of the Semi-analytical Method, for Determining the Geometrically non-Linear Response of thin Straight Structures: Part II First and Second Non-linear Mode Shapes of Fully Clamped Rectangular Plates," Journal of Sound and Vibration, vol. 257, no. 1, pp. 19–62, 2002. [CrossRef] [Google Scholar] [Publisher Link]
[32] M. El Kadiri, and R. Benamar, "Improvement of the Semi-analytical Method, Based on Hamilton's Principle and Spectral Analysis, for Determination of the Geometrically Non-linear Response of Thin Straight Structures. Part III: Steady State Periodic Forced Response of Rectangular Plates," Journal of Sound and Vibration, vol. 264, no. 1, pp. 1-35, 2003. [CrossRef] [Google Scholar][Publisher Link]
[33] K. El Bikri, R. Benamar, and M. Bennouna, "Geometrically Non-linear Free Vibrations of Clamped Simply Supported Rectangular Plates. Part I: The Effects of Large Vibration Amplitudes on the Fundamental Mode Shape," Computers & Structures, vol. 81, no. 20, pp. 2029–2043, 2003. [CrossRef] [Google Scholar] [Publisher Link]
[34] K. El Bikri, R. Benamar, and M.M. Bennouna, "Geometrically Non-linear Free Vibrations of Clamped–clamped Beams with an Edge Crack," Computers & Structures, vol. 84, no. 7, pp. 485–502, 2006. [CrossRef] [Google Scholar] [Publisher Link]
[35] Z. Beidouri, R. Benamar, and M. El Kadiri, "Geometrically Non-linear Transverse Vibrations of C–S–S–S and C–S–C–S Rectangular Plates," International Journal of Non-Linear Mechanics, vol. 41, no. 1, pp. 57–77, 2006. [CrossRef] [Google Scholar] [Publisher Link]
[36] Mohamed Haterbouch, and Rhali Benamar, "Geometrically Nonlinear free Vibrations of Simply Supported Isotropic thin Circular Plates," Journal of Sound and Vibration, vol. 280, no. 3-5, pp. 903–924, 2005. [CrossRef] [Google Scholar] [Publisher Link]
[37] B. Harras, R. Benamar, and R.G. White, "Geometrically Non-linear free Vibration of Fully Clamped Symmetrically Laminated Rectangular Composite Plates," Journal of Sound and Vibration, vol. 251, no. 4, pp. 579–619, 2002. [CrossRef] [Google Scholar] [Publisher Link]
[38] Lhoucine Boutahar, Khalid El Bikri, and Rhali Benamar, "A Homogenization Procedure for Geometrically Non-linear free Vibration Analysis of Functionally Graded Annular Plates with Porosities, Resting on Elastic Foundations," Ain Shams Engineering Journal, vol. 7, no. 1, pp. 313–333, 2016. [CrossRef] [Google Scholar] [Publisher Link]
[39] Zakaria Zergoune, Bilal Harras, and Rhali Benamar, "Nonlinear free Vibrations of C-C-SS-SS Symmetrically Laminated Carbon Fiber Reinforced Plastic (CFRP) Rectangular Composite Plates," World Journal of Mechanics, vol. 5, no. 2, pp. 20-32, 2015. [CrossRef] [Google Scholar] [Publisher Link]
[40] Mohcine Chajdi et al., "Linear and Geometrically Nonlinear free and Forced Vibrations of Multicracked Beams," Diagnostyka, vol. 20, no. 1, pp. 111-125, 2019. [CrossRef] [Google Scholar] [Publisher Link]
[41] Mohcine Chajdi et al., "Geometrically Nonlinear free and Forced Vibrations Analysis of Clamped-clamped Functionally Graded Beams with Multicracks," MATEC Web of Conferences, vol. 211, 2018. [CrossRef] [Google Scholar] [Publisher Link]
[42] Hatim Fakhreddine et al., "Geometrically Nonlinear free and Forced Vibrations of Euler-Bernoulli Multi-span Beams," MATEC Web of Conferences, vol. 211, 2018. [CrossRef] [Google Scholar] [Publisher Link]
[43] Ahmed Babahammou, and Rhali Benamar, "Geometrically Non-linear Free Vibrations of Simply Supported Rectangular Plates Connected to Two Distributions of Rotational Springs at Two Opposite Edges," Advances in Materials, Mechanics and Manufacturing, pp. 166–174, 2020. [CrossRef] [Google Scholar] [Publisher Link]
[44] Ahmed Babahammou, and Rhali Benamar, "Vibration Frequencies and Mode Shapes of CCFF Rectangular Plates Simply Supported at the Free Corner. Application to Large Vibration Amplitudes," Journal of Physics: Conference Series, vol. 1706, p. 012135, 2020. [CrossRef] [Google Scholar] [Publisher Link]
[45] Issam El Hantati et al., "A Multimode Approach to Geometrically Nonlinear Free and Forced Vibrations of Multistepped Beams," Shock and Vibration, 2021. [CrossRef] [Google Scholar] [Publisher Link]

[46] Adri Ahmed, and Benamar Rhali, "Geometrically Nonlinear Transverse Vibrations of Bernoulli-Euler Beams Carrying a Finite Number of Masses and Taking into Account Their Rotatory Inertia," Procedia Engineering, vol. 199, pp. 489-494, 2017. [CrossRef] [Google Scholar] [Publisher Link]
[47] O Outassafte et al., "Geometrically Nonlinear free Vibration of Euler-Bernoulli Shallow Arch," Journal of Physics: Conference Series, vol. 1896, p. 012013, 2021.[CrossRef] [Google Scholar] [Publisher Link]
[48] V. J. K. Silpa, B. V. S. Raghu Vamsi, and K. Gowtham Kumar, "Structural Analysis of thin Isotropic and Orthotropic Plates using Finite Element Analysis," SSRG International Journal of Mechanical Engineering, vol. 4, no. 6, pp. 13-24, 2017. [CrossRef] [Google Scholar] [Publisher Link]
[49] R. Benamar, "Nonlinear Dynamic Behavior of Fully Clamped Beams and Rectangular Isotropic and Laminated Plates," Southampton, 1990. [Google Scholar]
[50] Qingshan Wang, Dongyan Shi, and Xianjie Shi, "A Modified Solution for the Free Vibration Analysis of Moderately thick Orthotropic Rectangular Plates with General Boundary Conditions, Internal Line Supports and Resting on Elastic Foundation," Meccanica, vol. 51, pp. 1985–2017, 2016. [CrossRef] [Google Scholar] [Publisher Link]
[51] R. Benamar, M.M.K. Bennouna, and R.G. White, "The Effects of Large Vibration Amplitudes on the Mode Shapes and Natural Frequencies of Thin Elastic Structures, Part II: Fully Clamped Rectangular Isotropic Plates," Journal of Sound and Vibration, vol. 164, no. 2, pp. 295–316, 1993. [CrossRef] [Google Scholar] [Publisher Link]